1996

Investigation of Electrotribological and Arc Erosion Behavior of Cu-15vol.%Cr in situ Composite

Zhongyu Chen
Eastern Illinois University

THESIS REPRODUCTION CERTIFICATE

TO: Graduate Degree Candidates (who have written formal theses)

SUBJECT: Permission to Reproduce Theses

The University Library is receiving a number of requests from other institutions asking permission to reproduce dissertations for inclusion in their library holdings. Although no copyright laws are involved, we feel that professional courtesy demands that permission be obtained from the author before we allow theses to be copied.

PLEASE SIGN ONE OF THE FOLLOWING STATEMENTS:

Booth Library of Eastern Illinois University has my permission to lend my thesis to a reputable college or university for the purpose of copying it for inclusion in that institution's library or research holdings.

8-7-96
Date

I respectfully request Booth Library of Eastern Illinois University not allow my thesis to be reproduced because:

_____

_____

_____

_____ _____
Author Date

Investigation of Electrotribological and Arc Erosion Behavior of Cu-15vol.%Cr *in situ* Composite

(TITLE)

BY

Zhongyu Chen

THESIS

SUBMITTED IN PARTIAL FULFILLMENT OF THE REQUIREMENTS
FOR THE DEGREE OF

Master of Science in Technology

IN THE GRADUATE SCHOOL, EASTERN ILLINOIS UNIVERSITY
CHARLESTON, ILLINOIS

1996
YEAR

I HEREBY RECOMMEND THIS THESIS BE ACCEPTED AS FULFILLING
THIS PART OF THE GRADUATE DEGREE CITED ABOVE

8/1/96
DATE

8/1/96
DATE

THESIS COMMITTEE MEMBERS

8/1/96

Ping Liu, Ph.D., P.E., C.Q.E. and C.S.I.T. — Date
Professor
Thesis Adviser
School of Technology

Aug 96

Clifford E. Strandberg, Ed.D. — Date
Professor
Graduate Coordinator
School of Technology

8/1/96

Larry D. Helsel, Ed.D. and C.S.I.T — Date
Professor
School of Technology

Abstract

Electrotribological and arc erosion behavior of Cu-15vol.%Cr *in situ* composite was investigated in terms of coefficient of friction, interfacial resistance, bulk temperature, and wear rate as a function of normal pressure, sliding speed, and electrical current. Microstructural change due to electrical sliding was studied to understand wear mechanisms. Cu-15vol.%Cr *in situ* composite was selected in this research because it exhibits an excellent combination of mechanical strength and electrical/thermal conductivity.

It was found that the average coefficient of friction decreased with increasing electrical current under dry electrical sliding. The average coefficient of friction was lower under lubricated electrical sliding than that under dry electrical sliding, but it increased with increasing electrical current. There are no significant effects of normal pressure and sliding speed on coefficient of friction under dry electrical sliding. Under lubricated electrical sliding, the coefficient of friction decreased with increasing normal pressure, but it did not change significantly with sliding speed.

Both static and dynamic interfacial resistance decreased slightly with increasing normal pressure and the dynamic interfacial contact resistance decreased with increasing electrical current. The openness of circuit decreased with increasing normal pressure, increased with increasing sliding speed, and electrical current. The bulk temperature increased with increasing electrical current for both dry and lubricated electrical sliding.

The non-electrical wear rate of the composite increased with increasing normal

pressure and decreased with increasing sliding speed. The electrical wear rate decreased with increasing electrical current under dry electrical sliding, whereas the wear rate increased with increasing electrical current under lubricated electrical sliding. The effects of normal pressure and sliding speed on the wear rate of the composite under both dry and lubricated electrical sliding are dependent upon the level of electrical current.

The sliding-induced subsurface deformation occurred not only in the sliding direction but also in the lateral directions perpendicular to the sliding direction. The complex deformation mode was revealed clearly by the morphological change of the ribbon-like filaments. The thickness of the subsurface deformation layer increased with increasing normal pressure and sliding speed under dry non-electrical sliding. The thickness of the subsurface deformation layer decreased with increasing electrical current under dry electrical sliding, whereas the thickness increased with increasing electrical current under lubricated electrical sliding. A hardened surface layer and less damage on the subsurface layer were accounted for reduction in wear rate as electrical current was applied.

Acknowledgement

I would like to take this opportunity to express my sincerest appreciation and gratitude to Dr. Ping Liu for his guidance through the research and writing process. I would like to thank Dr. Clifford Strandberg and Dr. Larry D. Helsel serving as members of my thesis committee and for their advice and encouragement.

The research work was supported by the National Science Foundation under Grant No. MSS-9307797. The scanning electron microscopy was performed at the Center for Advanced Cement-Based Materials of the University of Illinois at Urbana-Champaign.

Thanks especially to my wife Mingxia and our daughter Diana for their support.

Table of Contents

CHAPTER 1

Introduction 1

1.1 Statement of the Research 2

1.2 Significance of the Research 2

1.3 Assumptions 2

1.4 Limitations 3

1.5 Delimitations 3

1.6 Hypothesis 4

1.7 Definitions 4

CHAPTER 2

Literature Review 6

2.1 Cu-Refractory *in situ* Composites 6

2.2 Tribological Behavior of Metal-Matrix Composites 9

2.3 Electrical Sliding Behavior 10

CHAPTER 3

Methodology 14

3.1 Materials 14

3.2 Wear Tests 15

3.3 Data Acquisition and Analysis 18

CHAPTER 4

Presentation and Interpretation of Data 21

4.1 Dry Non-Electrical Sliding of Cu-15vol.%Cr (Mode I) 21

4.1.1 Effect of Normal Pressure on Wear 21

4.1.2 Effect of Sliding Speed on Wear 23

4.1.3 Microstructural Change Due to Sliding 25
4.1.4 Thickness of Subsurface Layer 31
4.1.5 Wear Mechanism of Non-Electrical Sliding 33
4.2 Dry Electrical Sliding of Cu-15vol.%Cr (Mode II) 39
4.2 1 Effect of Electrical Current on Coefficient of Friction 39
4.2.2 Effects of Electrical Current on Bulk Temperature 40
4.2.3 Effect of Electrical Current on Wear 41
4.3 Lubricated Electrical Sliding of Cu-15vol.%Cr (Mode III) 43
4.3.1 Coefficient of Friction 43
4.3.2 Contact Behavior 45
4.3.2.1 Static contact resistance 45
4.3.2.2 Dynamic contact resistance 46
4.3.2.3 Openness of circuit under sliding 49
4.3.3 Bulk Temperature 51
4.3.4 Wear Rate 52
4.4 Microstructural Change during Electrical Sliding 55
4.4.1 Effect of Electrical Current on Thickness of Subsurface Layer . . . 58
4.4.2 Effect of Electrical Sliding on Microhardness 60
4.5 Wear Mechanism of Electrical Sliding 64

Conclusions 70

References 72

List of Figures

Figure		Page
1	Schematic diagram of nomenclature definition for specimen sections, rolling direction and sliding direction.	15
2	Schematic of pin-on-disk wear tester.	17
3	Data acquisition system.	20
4	Variation of composite volume loss with sliding distance for dry non-electrical sliding at a speed of 3.70 m s^{-1}.	21
5	Variation of wear rate of the composite with sliding time for dry non-electrical sliding at a speed of 3.70 m s^{-1}.	22
6	Variation of wear rate with normal pressure for the Cu-15vol.%Cr composite slid at a sliding speed of 3.70 m s^{-1} under dry non-electrical sliding.	23
7	Variation of wear rate of the composite with sliding time under a normal pressure of 0.31 MPa for dry non-electrical sliding.	24
8	Variation of wear rate with sliding speed under a normal pressure of 0.31 MPa for dry non-electrical sliding.	24
9	Microstructure of as-processed the Cu-15vol.%Cr *in situ* composite. (a) face section; (b) longitudinal section; (c) transverse section.	26
10	Schematic of subsurface plastic deformation pattern of the Cu-15vol.%Cr composite due to sliding.	27
11	Microstructural change of the Cu-15vol.%Cr *in situ* composite pin after sliding against a hardened AISI 52100 disk at a speed of 3.70 m s^{-1} for 60 min under dry non-electrical sliding. (a)under a normal pressure of 0.06 MPa; (b) under a normal pressure of 0.44 MPa. The arrow indicates the sliding direction.	28
12	Matched micrographs of the Cu-15vol.%Cr *in situ* composite pin, after dry non-electrical sliding for 60 min at a speed of 3.7 m s^{-1} and under a normal pressure of 0.31 MPa. (a) face section; (b) longitudinal section. The arrow indicates the sliding direction.	29

13 Schematic model of spatial shape change in the ribbon-like Cr filament during sliding wear process. 30

14 Variation of thickness of subsurface deformation layer with normal pressure at a sliding speed of 3.7 m s^{-1} under dry non-electrical sliding. 32

15 Variation of thickness of subsurface deformation layer with sliding speed under a normal pressure of 0.31 MPa for dry non-electrical sliding. 32

16 Schematic crystal deformation model for the Cu-15vol.%Cr *in situ* composite. 34

17 SEM micrograph revealed plastic deformation flow, after dry non-electrical sliding for 30 min at a speed of 3.7 m s^{-1} and under a normal pressure of 0.31 MPa. The arrow indicates the sliding direction. 35

18 Embedded wear debris inhibited the plastic deformation flow. The arrow indicates the sliding direction. 36

19 Transfer films on the steel disk for dry non-electrical sliding. (a) the original disk surface; (b) sliding direction normal to the ground groves and (c) sliding direction parallel to the ground groves of the steel disk, sliding at 3.70 m s^{-1} under a normal pressure of 0.06 MPa. The arrow indicates the sliding direction. 37

20 Variation of average coefficient of friction with electrical current for the Cu-15vol.%Cr under dry electrical sliding. 39

21 Variation of average bulk temperature with electrical current for the Cu-15vol.%Cr under dry electrical sliding. 40

22 Variation of wear rate with electrical current for the Cu-15vol.%Cr slid under dry conditions. 42

23 Variation of coefficient of friction with normal pressure for lubricated electrical sliding at a speed of 3.87 m s^{-1}. 44

24 Variation of coefficient of friction with sliding speed for lubricated electrical sliding under a normal pressure of 0.62 MPa. 44

25 Variation of coefficient of friction with electrical current for lubricated electrical sliding under a normal pressure of 0.62 MPa. 45

26 Variation of static interfacial resistance with normal pressure for dry and lubricated conditions. 46

27 Variation of dynamic interfacial resistance with normal pressure for lubricated electrical sliding at a speed of 3.87 m s^{-1}. 47

28 Variation of dynamic interfacial resistance with sliding speed for lubricated electrical sliding under a normal pressure of 0.62 MPa. 48

29 Variation of dynamic interfacial resistance with electrical current for lubricated electrical sliding under a normal pressure of 0.62 MPa. 48

30 Variation of openness of circuit with normal pressure for lubricated electrical sliding at a speed of 3.87 m s^{-1}. 49

31 Variation of openness of circuit with sliding speed for lubricated electrical sliding under a normal pressure of 0.62 MPa. 50

32 Variation of circuit openness with electrical current for lubricated sliding under a normal pressure of 0.62 MPa. 51

33 Variation of bulk temperature with electrical current for lubricated sliding under a normal pressure of 0.62 MPa. 52

34 Variation of wear rate with normal pressure for lubricated electrical sliding at a speed of 3.87 m s^{-1}. 53

35 Variation of wear rate with sliding speed for lubricated electrical sliding under a normal pressure of 0.62 MPa. 54

36 Variation of wear rate with electrical current for lubricated electrical sliding under a normal pressure of 0.62 MPa. 55

37 Face section microstructures of the Cu-15vol.%Cr *in situ* composite, (a) after dry electrical sliding; (b) enlarged view of interfacial microstructure in (a); (c) after lubricated electrical sliding. Arrow shows sliding direction. 56

38 SEM micrograph showed three-layer microstructural feature after lubricated electrical sliding. The Cu matrix was deeply etched. Arrow shows sliding direction. 58

39 Variation of subsurface deformation layer thickness with electrical current for the Cu-15vol.%Cr under electrical sliding. 59

40 Variation of microhardness for the Cu-15vol.%Cr with the distance from the sliding interface after dry sliding for 60 min under a normal pressure of 0.31 MPa and at a speed of 4.16 m s^{-1}, (a) non-electrical sliding; (b) electrical sliding under an electrical current of 50 A. 61

41 Variation of microhardness for the Cu-15vol.%Cr with the distance from the sliding interface after lubricated electrical sliding for 60 min under a normal pressure of 0.62 MPa and at a speed of 3.87 m s^{-1}. 63

42 Electrical arc eroded surface of the Cu-15vol.%Cr, after dry electrical sliding for 60 min under a normal pressure of 0.31 Mpa, at a speed of 4.16 m s^{-1}, and under an electrical current of 50 A. Arrow shows the sliding direction. 64

43 SEM micrographs of the Cu-15vol.%Cr, after dry electrical sliding for 60 min under a normal pressure of 0.31 MPa, at a speed of 4.16 m s^{-1}, and under an electrical current of 40 A. (a) surface crack; (b) arc eroded pits, and (c) wear debris attached on the surface. Arrow shows the sliding direction. 65

44 Wear debris collected from a dry electrical sliding test under a normal pressure of 0.31 MPa, at a speed of 3.33 m s^{-1}, and under an electrical current of 30 A. 67

45 Electrical arc eroded wear surface of the hardened steel disk, after dry electrical sliding for 60 min under a normal pressure of 0.31 MPa, at a speed of 4.16 m s^{-1}, and under an electrical current of 10 A. Arrow shows the sliding direction. 68

CHAPTER 1

Introduction

The efficient utilization of energy and increasing operational velocity of electrical machines demand that electrical contact materials have superior resistance to wear and arc erosion. Homopolar machines, for example, which were developed for efficient propellers of large ships and for pulsed power applications, operate at a linear sliding speed up to 200 m s^{-1} and an electrical current density of 20 MA m^{-2} (McNab, 1980; Persad *et al.*, 1990). The high speed and high electrical current density cause severe wear and arc erosion on conventional electrical contact materials. New electrical contact materials are being developed to meet the challenges under these severe operating conditions.

Among the new materials for electrical contact applications, copper-refractory *in situ* composites are promising because of their superior combination of high mechanical strength and high electrical/thermal conductivity (Verhoeven *et al.*, 1990). Cu-15vol.%Cr *in situ* composite was selected in this research, not only because it exhibits an excellent combination of high strength and high electrical/thermal conductivity, but also because Cr offers such features as lower cost, better corrosion resistance, and higher modulus of elasticity than other refractory elements. A fundamental understanding of electrical sliding behavior and arc erosion of the composite will facilitate the material development and tribological applications.

1.1 Statement of the Research

Electrotribological and arc erosion behavior of Cu-15vol.%Cr *in situ* composite was investigated in terms of coefficient of friction, wear rate, and bulk temperature as a function of normal pressure, sliding speed, and electrical current. The microstructural change due to electro-mechanical sliding was studied to understand wear mechanisms. Cu-15vol.%Cr *in situ* composite was selected in this research because it exhibits an excellent combination of mechanical strength and electrical/thermal conductivity.

1.2 Significance of the Research

Cu-15vol.%Cr *in situ* composite was developed as promising electrical contact materials to meet the challenges of their severe operating conditions in electrical machines of high speed and high current. The composite has superior properties in terms of mechanical strength and electrical conductivity. A fundamental understanding of its electrotribological and arc erosion behavior will facilitate the material development and promote its tribological applications such as vehicle propulsion, inertial storage pulsed power generators, and electromagnetic projectile launchers.

1.3 Assumptions

Wear behavior of Cu-15vol.%Cr *in situ* composite can be investigated by a pin-on-disk tester.

Wear behavior of Cu-15vol.%Cr *in situ* composite is correlated to normal pressure, sliding speed, and electrical current.

Wear mechanisms can be understood by analyzing coefficient of friction, bulk temperature rise, wear rate, and microstructural change.

1.4 Limitations

The following factors which may influence tribological behavior of Cu-15vol.%Cr *in situ* composite are not controlled and the findings of the study were limited by the following parameters.

Room temperature and relative humidity may change during study.

Property uniformity of copper-refractory *in situ* composite and steel disk may vary.

1.5 Delimitations

The study was delimitated by the following parameters.

Cu-15vol.%Cr *in situ* composite was used as sliding pin, with a cross-section area of 15.7 mm^2 and a hardness of 74 RB.

AISI 52100 steel was used as disk that had hardness between 58.5 and 62 RC after heat treatment.

Surface finish was determined by surface grinding for the steel disks and by grinding on Carbimet® papers up to grit 600 in running water for the composite pins.

Normal pressure was in the range of 0.06 - 0.75 MPa.

Sliding speed varied from 2.32 to 5.56 m s^{-1}.

Electrical current was between 0 and 50 A while pin was connected as cathode.

SAE 10 motor oil was used as a lubricant.

Total testing length was 60 min.

1.6 Hypothesis

Normal pressure, sliding speed, electrical current density, and lubrication can significantly affect electrotribological behavior in terms of coefficient of friction, wear rate, and bulk temperature.

1.7 Definitions

Arc erosion: Damage to the surfaces of electrical contacts where a narrow gap exists and electrical discharge occurs. Arc erosion usually results in high temperature and local melting of electrical contacts.

Bulk temperature: An average temperature of a sliding pin caused by friction heating and/or joule heating during electrical sliding.

Coefficient of friction: The ratio of friction force, F, to the normal load, N, pressing the two bodies together. It refers to dynamic coefficient of friction when sliding is in process.

Cu-15vol.%Cr *in situ* composite: A metallic matrix composite, made by casting followed by extensive cold deformation. The composite has an excellent combination of high mechanical strength and electrical/thermal conductivity.

Filaments/Ribbons: Interchangeable terms used for the Cr phase in the Cu-Cr *in situ* composite.

Normal pressure: A normal load per unit contact area of a sliding pin.

Plastic deformation: A permanent deformation caused by dislocation movement.

Sliding speed: Relative speed of a sliding pin against a disk.

Thickness of subsurface deformation layer: A thickness measured on a worn specimen, including plastic deformation zone, refined zone and surface film.

Wear: Damage to a surface as a result of relative motion with respect to another substance. Materials are either removed as wear debris or deformed on the surface and subsurface.

CHAPTER 2

Literature Review

A composite is a material having two or more distinct constituents, *i.e.*, its matrix and reinforcements. Composites can be classified into ceramic, metallic and polymeric matrix composites. Metal matrix composites are completely new materials that have only been developed since 1960's (Matthews & Rawlings, 1994).

Metal matrix composites, with other advanced composites, offer the capability of tailoring the properties of materials to meet the requirements of a design. By selectively adding reinforcements to a metal matrix, such properties as strength, stiffness, thermal expansion, wear resistance, and electrical conductivity can be adjusted and improved. Reinforcements may be continuous or discontinuous fibers, particles or whiskers. Metallic reinforcements are used when compatibility between a matrix and a reinforcement and processing costs become a main concern.

Although metallic matrix composites are still in their initial stage of development and some phenomena involved remain unknown, they are widely used in such products as automobiles, airplanes, and sporting goods. Because composites can be tailored to specific property requirements, new application doors will continue to open.

2.1 Cu-Refractory *in situ* Composites

A composite is known as *in situ* composite if its morphology is directly produced during the manufacturing (Courtney, 1991). The heavily deformed *in situ* composites can be prepared by means of powder metallurgy (Pourrahimi, Nayeb-Hashemi, & Foner,

1992) or by quenching a liquid solution (Verhoeven, Gibson, Schmidt, & Finnemore, 1980). Verhoeven *et al.* reported two techniques, chill casting and consumable arc melting, for preparing Cu-Nb ingots.

Several mutually soluble systems such as Cu-Fe, Ag-Fe, and Ag-28.2wt.%Cu (Frommeyer & Wassermann, 1975) *in situ* composite wires were first investigated in Germany by means of extensive cold deformation with a reduction of cross-section up to 99.999%. It was found that the average diameter of metal fibers decreased with increasing reduction of cross-section and the tensile strength of these composite wires were well above the values predicted by the rule of mixture. Very fine metal fibers (12.5 nm) resulted from an area reduction of 99.995%.

Cu-Nb system was first studied as an A-15 superconducting wire because of superconductivity of Nb_3Sn-Cu and for its anomalous increase in strength (Bevk, Harbison, & Bell, 1978; Renaud, Gregory, & Wong, 1988). Because Nb has a very low solid solubility in the Cu matrix at room temperature (ASM, 1992), the microstructure of the Cu-Nb *in situ* composite consists of pure Nb filaments and nearly pure Cu matrix. Bevk *et al.* reported that the ultimate strength of most highly reduced wires was comparable to the estimated theoretical strength of the material and was as high as that of the Cu whisker, retaining high electrical/thermal conductivity (60% of pure copper). An excellent combination of mechanical strength and electrical/thermal conductivity from those *in situ* composites can be reached by the extensive cold deformation technique. Renaud *et al.* reported that a new world record for the highest magnetic field ever generated by a wire wound solenoid of 68.4 T was made possible with Cu-18Nb *in situ*

composite wires.

Since then, Cu-Nb *in situ* composites have attracted many research efforts because of the resultant superior combination of electrical/thermal conductivity and mechanical strength (Spitzig & Krotz, 1987; Spitzig, Pelton, & Laabs, 1987; Verhoeven, Spitzig, Schmidt, Krotz, & Gibson, 1989; Trybus & Spitzig, 1989; Chumbley, Downing, Spitzig, & Verhoeven, 1989; Spitzig & Reed, 1989; Verhoeven *et al.*, 1990; Verhoeven, Chumbley, Laabs, & Spitzig, 1991; Spitzig, Downing, Laabs, Gibson, & Verhoeven, 1993). Research was concentrated on mechanical properties, microstructure, and strengthening mechanisms. Emissivity of etched Cu-Nb *in situ* alloys (Downing, Verhoeven, & Gibson, 1987) and rolling texture (Raabe, Ball, & Gottstein, 1992) were studied.

In spite of the brittle nature of pure Cr at room temperature, the remarkable malleability of the isolated Cr phase in a Cu-17vol.%Cr alloy drawn into long filaments was first demonstrated (Funkenbusch, Courtney, & Kubisch, 1984; Funkenbusch & Courtney, 1985). Through appropriate control of the initial microstructure, the cast alloy could be drawn to a true strain of 6.3. The tensile strength of the Cu-17vol.%Cr *in situ* composite increased with increasing true drawing strain, reaching 840 MPa at a true drawing strain of 6.3 (Funkenbusch & Courtney), which was well above that predicted by the rule of mixtures.

The other reason of developing Cu-Cr deformation-processed *in situ* composite is that Cr offers lower cost, better corrosion resistance, and higher modulus of elasticity than Nb. Because Cu-15vol.%Cr alloy exhibited similar deformation characteristics as

Cu-Nb (Verhoeven *et al.,* 1990) and the strength of the composite was shown to increase with modulus of constituent, Spitzig *et al.* (1987) expected that Cr would produce higher strength at a given deformation strain.

Kim (1993) studied a Cu-7vol.%Cr *in situ* composite. A combination of a strength of 925 MPa and an electrical conductivity of 71.8 % IACS (International Annealed Copper Standard) was achieved. Annealing remarkably influenced the microstructure and the mechanical properties of a heavily deformed Cu-15vol.%Cr microcomposite sheet (Hardwick, Rhodes & Fritzemeier, 1993). Extensive spheroidization of the Cr ribbons occurred after annealing for ten hours at 650 °C. As a result, the yield strength was reduced by 55% and the ductility increased.

Systems other than Cu-Nb/Cr were also investigated, including Ni-W, Cu-Mo (Funkenbusch *et al.*, 1984), Cu-Ta (Spitzig & Krotz, 1988), Cu-Fe (Verhoeven, Chueh, & Gibson, 1989).

2.2 Tribological Behavior of Metal-Matrix Composites

Friction and wear behavior of metal-matrix composites has attracted considerable interest. Most of the composites are reinforced with nonmetallic fibers, particles or whiskers (Rohatgi, Liu, & Ray, 1993). No investigation of friction and wear behavior of Cu-Cr *in situ* composites is available. Some studies have been conducted for friction and wear behavior of Cu-Nb *in situ* composites.

Liu, Bahadur and Verhoeven (1993b) studied the effects of Nb composition and true deformation strain on coefficient of friction and wear rate. A Cu-Nb *in situ*

composite pin was slid against a hardened O2 tool steel disk at sliding speeds from 0.028 to 2.5 m s^{-1} and under a normal pressure of 0.68 MPa. It was found that Cu-20vol.%Nb showed the best wear resistance. Increasing true deformation strain resulted in increased tensile strength and coefficient of friction, and decreased wear rate. The tribological behavior of the Cu-20vol.%Nb *in situ* composite was investigated in terms of sliding-induced plastic deformation flow, effects of Nb filament orientation, sliding speed and annealing temperature (Liu, Bahadur, & Verhoeven, 1993a). The wear rate of the specimen with Nb filaments perpendicular to the sliding direction was lower than that with Nb filaments parallel to the sliding direction, which indicated that this *in situ* composite had an anisotropic wear resistance as modeled by Hornbogen (1985). With increased annealing temperature, the hardness of the composite decreased, and both the coefficient of friction and the wear rate increased. It was found that both the Cu matrix and Nb filaments underwent sliding-induced deformation with no loss of bonding between the Nb filaments and the Cu matrix. Increasing sliding speed resulted in a lower wear rate, which was ascribed to oxidation and work hardening.

Nayeb-Hashemi and Lee (1993) investigated the friction and wear behavior of powder metallurgical Cu-Nb microcomposite rubbing against grey cast iron of hardness 92 RB. They found that the wear rate increased drastically with sliding speed and the coefficient of friction was independent of fiber orientations.

2.3 Electrical Sliding Behavior

Johnson and Schreurs (1982) studied contact resistance using a probe embedded

in the brush approximately 1.6 mm from the sliding surface and they claimed in this way only constriction resistance was included. They found that the contact resistance varied considerably for a given brush polarity and current density. Contact resistance at the anode brush was higher than that at the cathode brush. With increasing current density, contact resistance first increased, then decreased, and increased to dusting. Contact resistance at the cathode brush remained virtually constant but the contact resistance at the anode brush increased with time. When the polarity was reversed, the new cathode resistance initially dropped rapidly and then decreased more slowly to a value close to that of the original cathode. At the new anode, the contact resistance rose slowly, which was similar to the increase observed at the original anode brush. When current density increased, the coefficient of friction decreased and the wear rate increased.

Myshkin and Konchits (1992) studied self-lubricating composites for current collection and wear resistance. The composites of metal-graphite, carbon-graphite, and electrographite were made by powder metallurgy. The brush noise and the brush friction against the collector decreased with increasing electrical current for the traditional electrobrush materials. For metallic brush there is no such "current lubrication".

Donaldson, Lehr, and Christiansen (1988) studied switches sustaining current densities of 10 GA m^{-2}. Electrode erosion was expressed as $V_e = k_v V_v + k_l V_l$, where subscripts v and l represent vapor and liquid, respectively. Coefficients k_v and k_l have been shown to be a function of the high temperature strength of the material, and/or the ability of the two constituent materials to retain the lower melting point material in the liquid state until evaporation occurs. The volumes V_v and V_l were determined as a

function of the arc current by solving the heat conducting equation. They stated that Cu-Nb *in situ* composites and the addition of the LaB_6 might yield improved contact performance and lower arc erosion.

Liu, Bahadur, and Verhoeven (1994) studied the friction and wear behavior of Cu-Nb *in situ* composites when electrical current was passed between the sliding interface. The effects of Nb proportion, electrical current density, sliding speed, and Nb filament orientation on friction and wear behavior were investigated. It was found that both the coefficient of friction and the wear rate decreased at higher sliding speed when an electrical load was applied. In addition, the temperature rise in electrical sliding contact from electrical Joule heating helped the formation of surface oxide film.

Temperature rise may be symmetric, *i.e.*, maximum temperature occurs in the interface, or asymmetric, *i.e.*,maximum temperature may occur in brush if it has low electrical and thermal conductivity (McNab, 1980). Temperature rise due to friction is proportional to the coefficient of friction, the normal force, and the relative speed. The coefficient of friction is determined by both solid and adsorbed films.

Schreurs, Johnson, and McNab (1980) used low energy electron diffraction to investigate surface film within one to ten atomic layers of the gas-solid interface. The silver-graphite brush was slid against a Cu slip ring of machined surface at 13 m s^{-1} under 0.75 MA m^{-2} current density, CO_2 atmosphere with 0.01 molecular percent H_2, with added water vapor to a dew point of 20 °C. The friction, wear, and electrical properties of the sliding system are controlled by the thin film, surface microtopography, hardness, applied force on the sliding members, the cohesive forces between the two metals in

contact, and the relative strength of the interfaces in the brush and slip ring.

Lubricants were applied in electrical sliding contacts for smooth operation, reduced friction and noise, and prolonged service (Okada, Baba, & Yoshida, 1989; Lysonski *et al.*, 1990). Lysonski *et al.* found a family of halogenated aryl ester fluids could provide significantly reduced friction and wear on sliding gold electrical contacts. These halogenated aryl esters could be effectively used either as pure lubricant or as additives and are soluble in most fluorocarbons and halocarbons.

Okada *et al.* (1989) tested a combination of silicon oil and Vaseline with ultra fine Ag-30%Pd alloy powders for copper brushes on a flat 18-8 stainless steel slip ring. It was found that contact resistance for the sliding brush would become larger than that for the stationary brush when a film of lubricant separated the brush and the ring. When real contact occurred, contact resistance decreased with increasing load and increased with increasing current.

Sliding contact and arcing characteristics of brass against a steel disk were studied using an instrumentation capable of detecting circuit openness and arcing (Fujiwara, Tsukamoto, & Azakami, 1990). It was found that the frequency of openness for sliding contact increased with increased sliding speed and decreased with increased current. However, the frequency of arcing for sliding contact increased with increased sliding speed and current.

CHAPTER 3

Methodology

3.1 Materials

A Cu-15vol.%Cr alloy ingot was first smelted by the vacuum induction melting method, then cast to make an electrode for the subsequent consumable electrode arc melting to obtain uniform and fine Cr dendrites in the Cu matrix. The deformation process started with the hot extrusion of an ingot of 101.6 mm in diameter into a rod of 50.8 mm in diameter. The rod was rolled into a plate of 12.7 mm thick and finally into a sheet of 1.59 mm thick. The true deformation strain was 5.4 or the area reduction rate 99.5% for the Cu-15vol.%Cr.

The Cu-15vol.%Cr *in situ* composite sheet thus processed had a microstructure of ribbon-like Cr filaments aligned in the rolling direction. The definition of the composite specimen sections and the relationship between the rolling direction and the sliding direction are illustrated in Fig. 1.

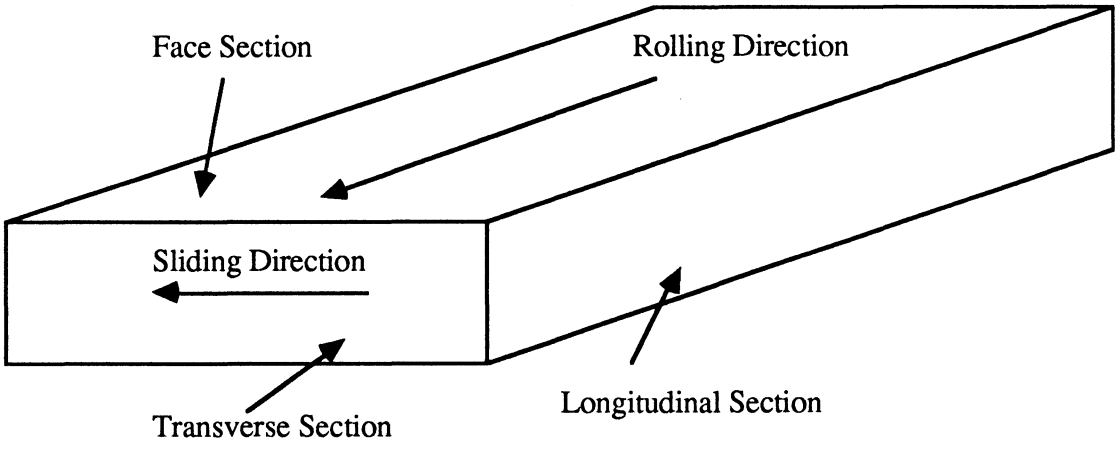

Figure 1. Schematic diagram of nomenclature definition for specimen sections, rolling direction and sliding direction.

3.2 Wear Tests

Sliding tests were performed on a pin-on-disk wear tester, with a Cu-15vol.%Cr *in situ* composite pin rubbing against a hardened AISI 52100 steel disk. The tests were classified into three modes, as listed in Table 1. In mode I, a composite pin was slid under dry non-electrical sliding and weighed every five minutes with total sliding time of 60 min. In mode II, a composite pin was slid continuously for 60 min under dry conditions with electricity applied across the sliding interface between the composite pin and the steel disk. After the sliding test of 60 min was completed, the specimen was weighed. In mode III, a lubricant was added in the electrical sliding.

Table I

Three Sliding Modes Used in this Research

Mode	Timing	Electricity	Lubrication
I: Dry non-electrical sliding	5 min interval, total 60 min	No	No
II: Dry electrical sliding	60 min continuously	Yes	No
III: Lubricated electrical sliding	60 min continuously	Yes	Yes

The pins were cut from a heavily deformed Cu-15vol.%Cr sheet and had a rectangular transverse section of 1.57 x 10 mm. During a wear test, the ten-millimeter length of the specimen was in the sliding direction and the Cr filaments perpendicular to the sliding interface. The steel disk was austenitized at 843 °C for 30 min, oil quenched, and tempered at 150 °C for 60 min. The hardness of the disk was 60 RC. The hardness for the Cu-15vol.%Cr *in situ* composite pins was 74 RB.

A modified pin-on-disk wear tester was used for the electrical sliding tests under lubricated conditions. Figure 2 shows the main part of the wear tester. About ten milliliters of non-detergent motor oil (SAE 10) were used as a lubricant. The oil bath was rotated with the disk and the lubricant was kept by a plastic cover and seal rubber.

Before a sliding test, the composite pin was ground on a Carbimet® paper to grit 600 on a Handimet® grinder in running water, and then cleaned in methyl alcohol for five minutes using an ultrasonic cleaner. The disks with surface roughness (R_a) of 0.20 μm were cleaned with methyl alcohol. The composite pin was weighed every five minutes for mode I or 60 min for other two modes with an accuracy of 10^{-7} N. The sliding speed

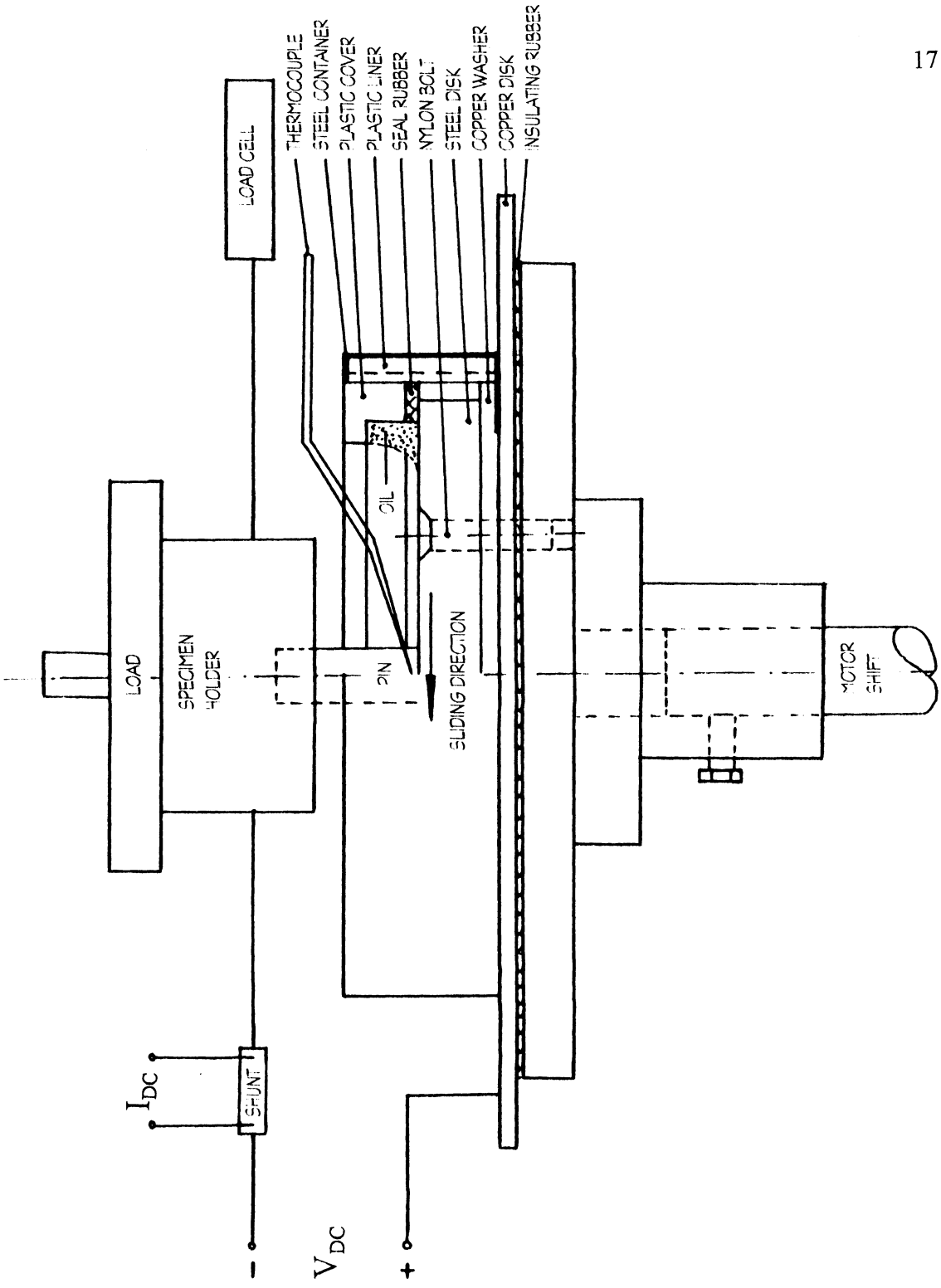

Figure 2. Schematic of pin-on-disk wear tester.

varied from 2.78 to 6.49 m s^{-1} and the normal pressure varied from 0.06 to 0.72 MPa.

The pin holding arm was free to rotate in both vertical and sliding directions to facilitate friction force measurement. The pin holder was connected by flexible nylon lines with a full bridge thin-beam load cell. To measure the temperature on the composite pin, a thermocouple was inserted in a hole of 0.7 mm in diameter in the composite pin and located 1.5 mm above the sliding interface.

An electrical current from a DC power source in constant current mode was applied across the sliding interface between a composite pin and a steel disk. The composite pin was connected as the cathode and the disk as the anode. The electrical current varied between 0 and 50 A and the maximum voltage was controlled at 12 V for the dry electrical sliding and 4.5 V for the lubricated electrical sliding.

Electrical current (I_{DC}) flowing through the interface was measured using a shunt resistor of 0.25 mΩ (50 mV at 200 A). By measuring the voltage across the shunt resistor, the electrical current was calculated by the formula, $I_{DC} = \frac{V_{Shunt}\ (mV)}{0.25}$. Contact behavior was studied by means of openness of circuit defined as a status when the interfacial voltage was higher than 3.5 V. One openness of circuit lasted 1/2000 s or 0.5 μs. Percentage of circuit openness was used in the final presentation.

3.3 Data Acquisition and Analysis

Two data acquisition systems were used in this research. One consisted of an eight-channel interface (ADC 1556E-8D) and a 286 personal computer. Because the scanning rate of the system was relatively slow, it was mainly used for sliding mode I and

II. Through the eight-channel interface, coefficient of friction and bulk temperature were recorded in the microcomputer every four seconds. Data from the eight-channel interface needed to be transformed into the format that could be used by a software (PSIPLOT) for further analysis.

The other data acquisition system had a scanning rate as high as 20,000 scans per second for each channel. The schematic for the system is shown in Fig. 3, which was used for acquiring data for sliding mode III to investigate sliding contact characteristics. All four parameters, *i.e.*, friction force, bulk temperature, electrical current, and interface voltage were measured, processed, and recorded by the microcomputer and LabView program. A scanning rate of 2000 scans per second was used for each channel. To reduce noise, an average of 1000 measuring points was used to represent a datum point. Totally, 7200 data points were recorded for each parameter in each test.

Microhardness was measured with Micromet® 2001 microhardness tester, using Vickers indenter under a load of 0.098 N and for a dwell time of ten seconds. Surface roughness (R_a) was measured with Surfcom 120A, using the following parameters:

Stylus	01
Vertical magnification (Vv)	4000
Horizontal magnification (Vh)	20
Measuring length (L)	4 mm
Cutoff value (λ_c)	0.8 mm

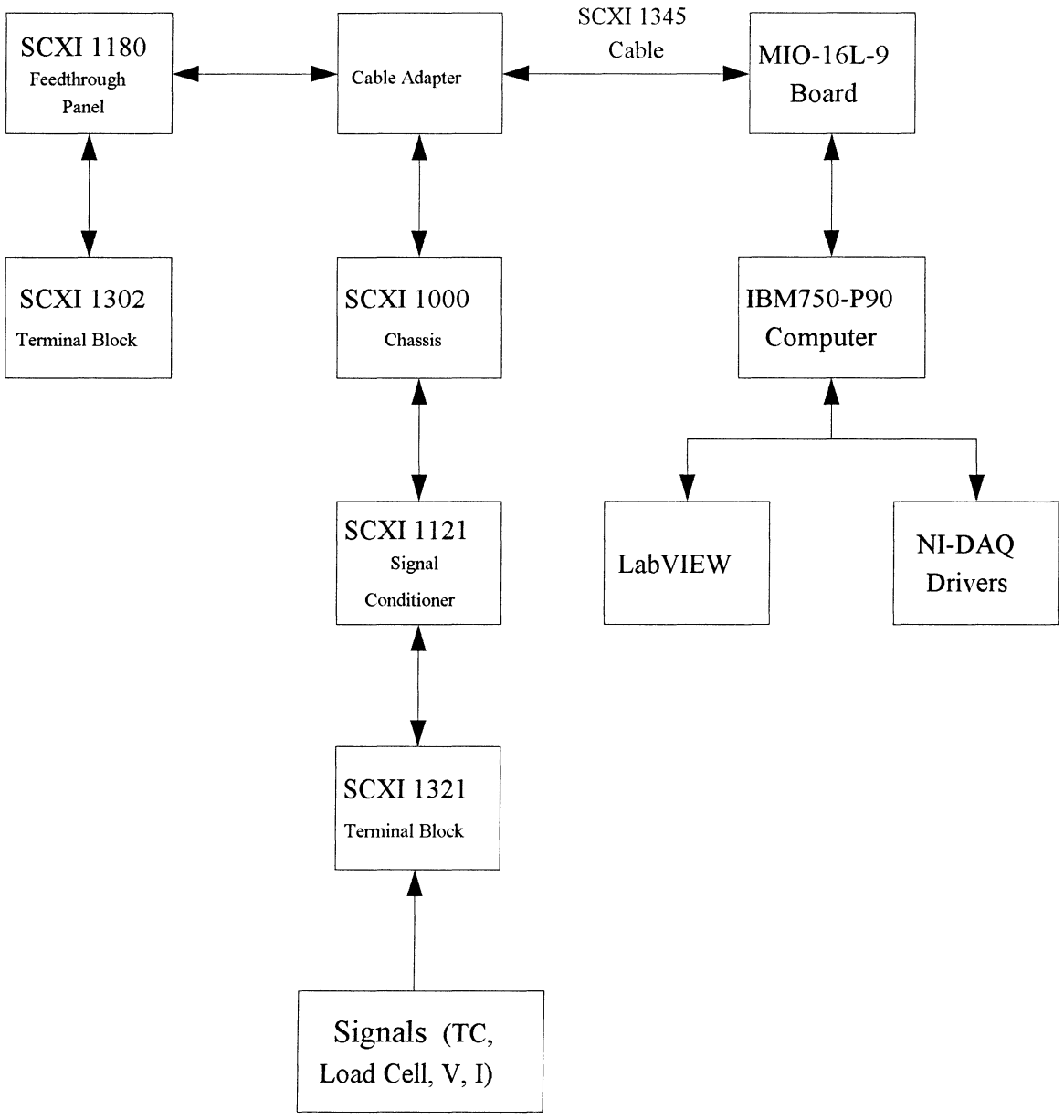

Figure 3. Data acquisition system.

CHAPTER 4

Presentation and Interpretation of Data

4.1 Dry Non-Electrical Sliding of Cu-15vol.%Cr (Mode I)

4.1.1 Effect of Normal Pressure on Wear

The variation of volume loss of the Cu-15vol.%Cr *in situ* composite with sliding distance at a sliding speed of 3.70 m s^{-1} is shown in Fig. 4. The volume loss increased with increasing sliding distance, with a rapid increase during the running-in stage and an almost linear increase in the following steady-state stage. Under a normal pressure of 0.44 MPa, the total volume loss was much greater than that under lower normal pressures.

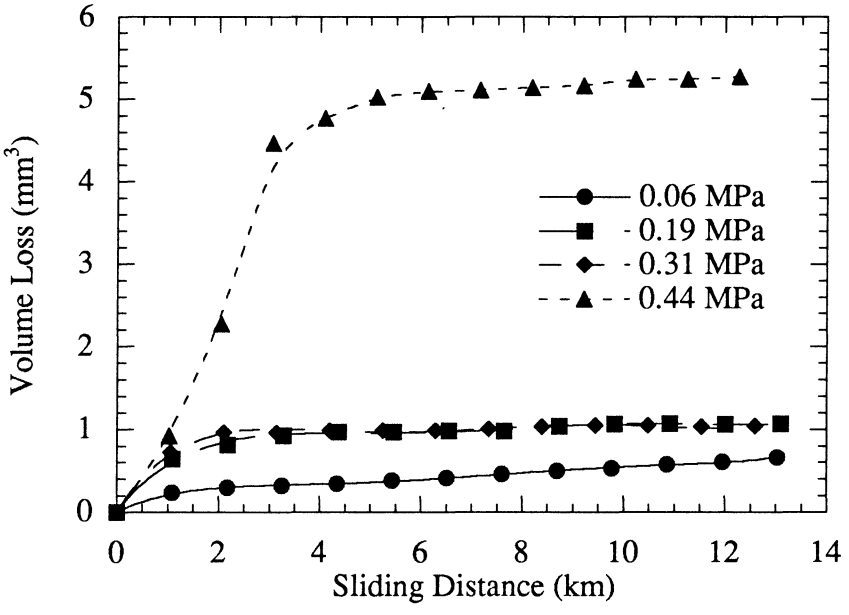

Figure 4. Variation of composite volume loss with sliding distance for dry non-electrical sliding at a speed of 3.70 m s^{-1}.

Wear rate is defined as total volume loss per sliding distance (Rigney, 1988). The variation of the wear rate with sliding time is illustrated in Fig. 5. The wear rate decreased with sliding time, approaching a steady state. It may be seen in Figs. 4 and 5 that increasing the pressure from 0.31 to 0.44 MPa produced a sharp increase in the wear rate. This transition is illustrated clearly in Fig. 6 that plots the wear rate as a function of normal pressure. It is seen that a sharp transition from a mild wear to a severe wear occurred when the pressure increased from 0.31 to 0.44 MPa. These data show that the material should be maintained at a normal pressure below 0.44 MPa to avoid severe wear while sliding at a speed of 3.7 m s^{-1} under dry non-electrical sliding.

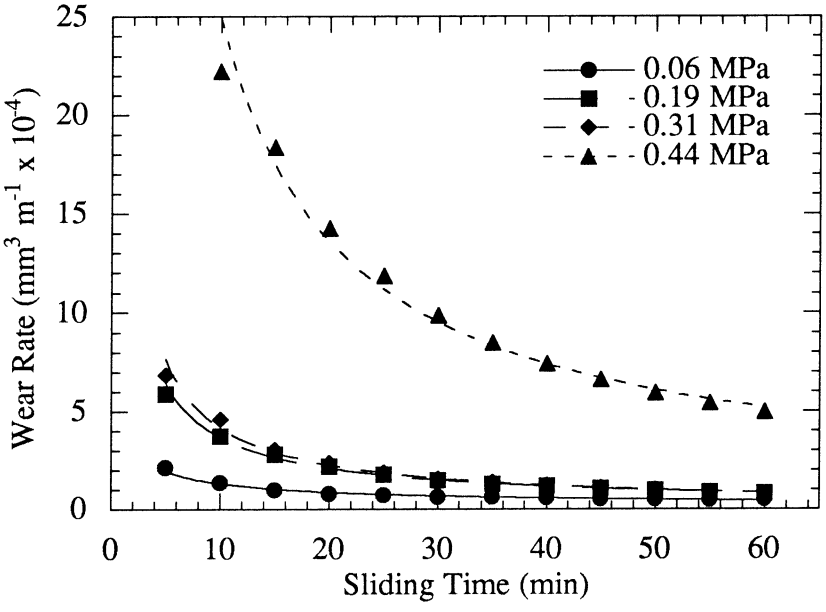

Figure 5. Variation of wear rate of the composite with sliding time for dry non-electrical sliding at a speed of 3.70 m s^{-1}.

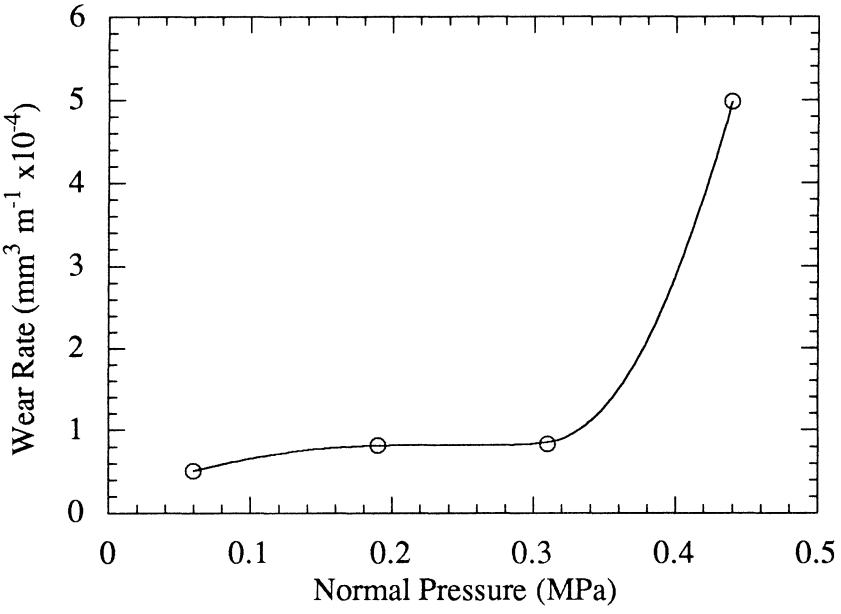

Figure 6. Variation of wear rate with normal pressure for the Cu-15vol.%Cr composite slid at a sliding speed of 3.70 m s^{-1} under dry non-electrical sliding.

4.1.2 Effect of Sliding Speed on Wear

The change of the wear rate with sliding time under a normal pressure of 0.31 MPa is shown in Fig. 7 for various sliding speeds. The wear rate decreased with sliding time at all sliding speeds. In general, a higher sliding speed was related to a lower wear rate. Figure 8 shows the variation of the wear rate with sliding speed under a normal pressure of 0.31 MPa. The wear rate decreased with increased sliding speed, but it tended to level off at a sliding speed of 4.63 m s^{-1}.

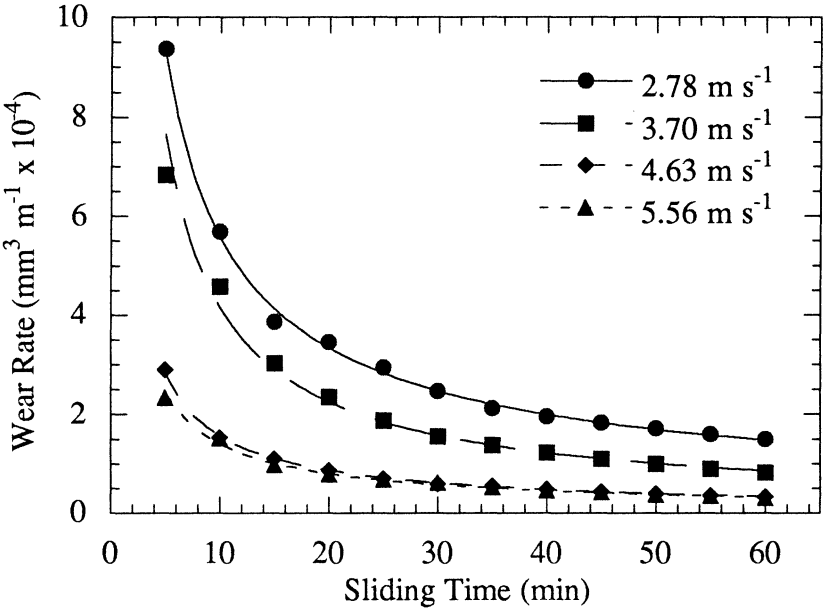

Figure 7. Variation of wear rate of the composite with sliding time under a normal pressure of 0.31 MPa for dry non-electrical sliding.

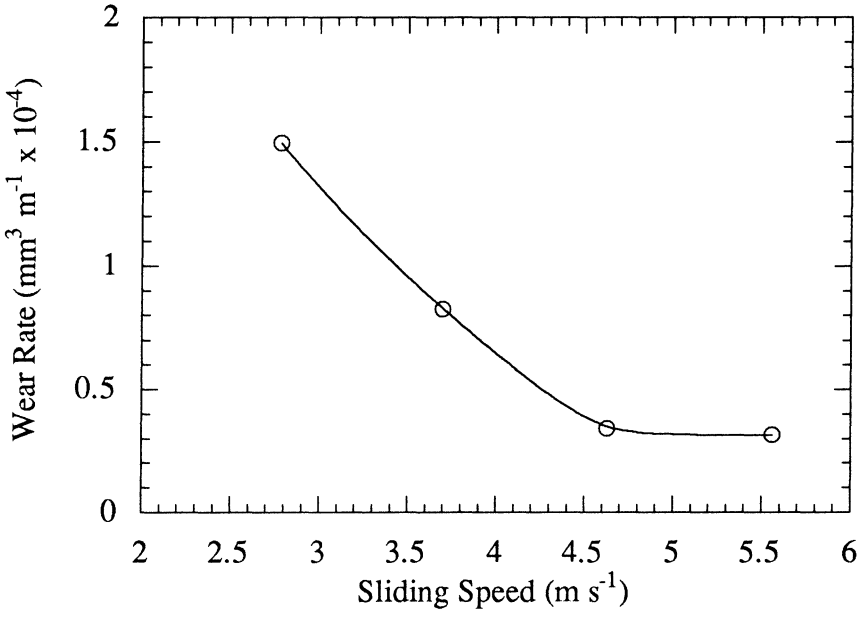

Figure 8. Variation of wear rate with sliding speed under a normal pressure of 0.31 MPa for dry non-electrical sliding.

4.1.3 Microstructural Change Due to Sliding

The microstructure of the Cu-15vol.%Cr *in situ* composite before sliding is shown in Fig. 9. Figure 9 (a) was taken on the face section, Fig. 9 (b) on the longitudinal section, and Fig. 9 (c) on the transverse section. The Cr filaments, with variable cross sections, align in the rolling direction. Figure 9 (b) illustrates that some Cr filaments with coarse knots are present in the longitudinal section. That is, Cr dendrites were not uniformly deformed into thin ribbons. Some Cr particles can also be seen as spherical precipitates in the Cu matrix.

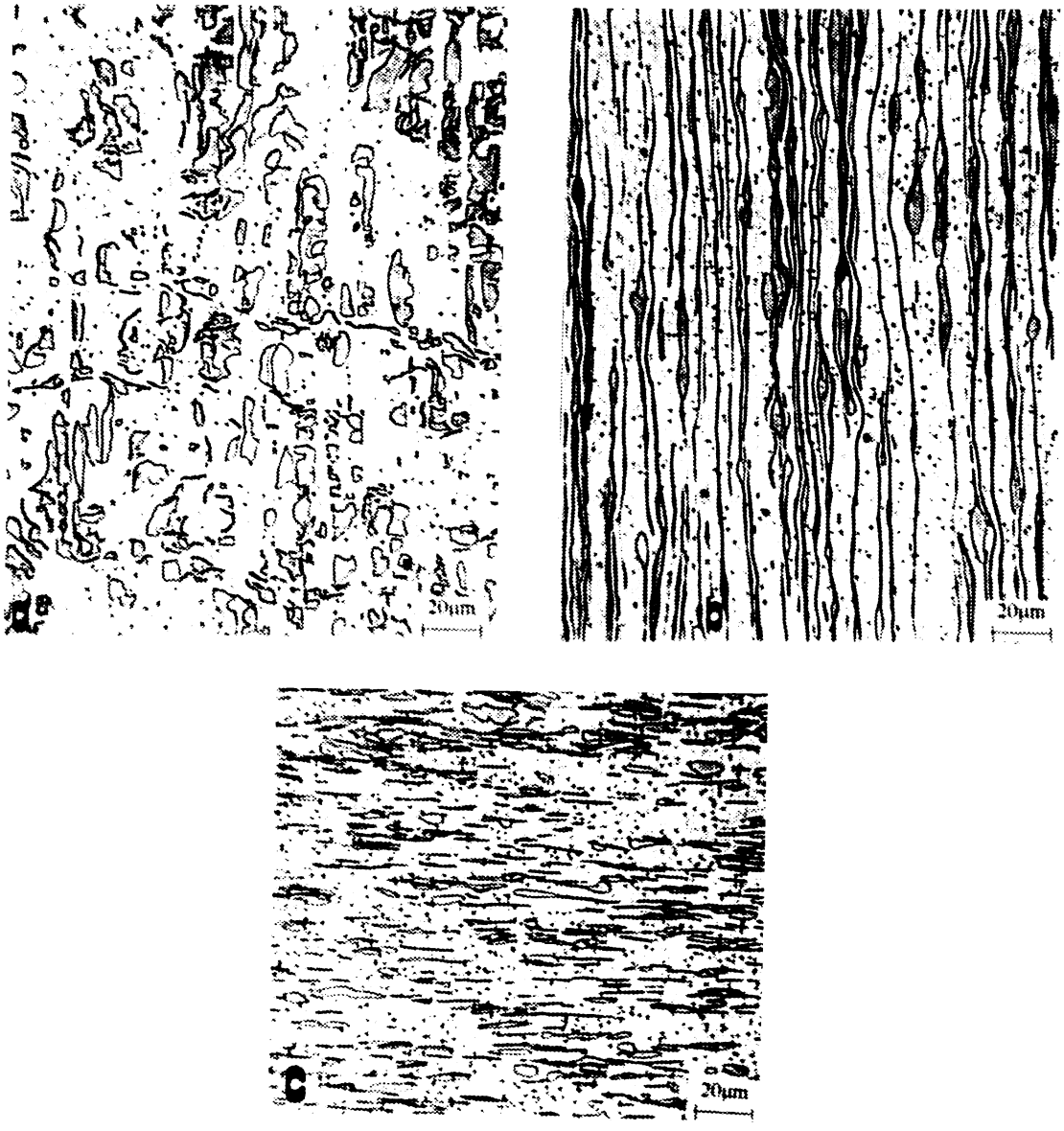

Figure 9. Microstructure of as-processed the Cu-15vol.%Cr *in situ* composite. (a) face section; (b) longitudinal section; (c) transverse section.

By studying the change in the Cr filament alignment near the worn surface, it was possible to evaluate the nature of the deformation layer produced at the surface. Figure 10 illustrates an ideal deformation pattern caused by sliding, which could be depicted by the change in the Cr filaments. The deformation layer had a maximum thickness at the faces of the pin, and the layer thickness decreased symmetrically toward

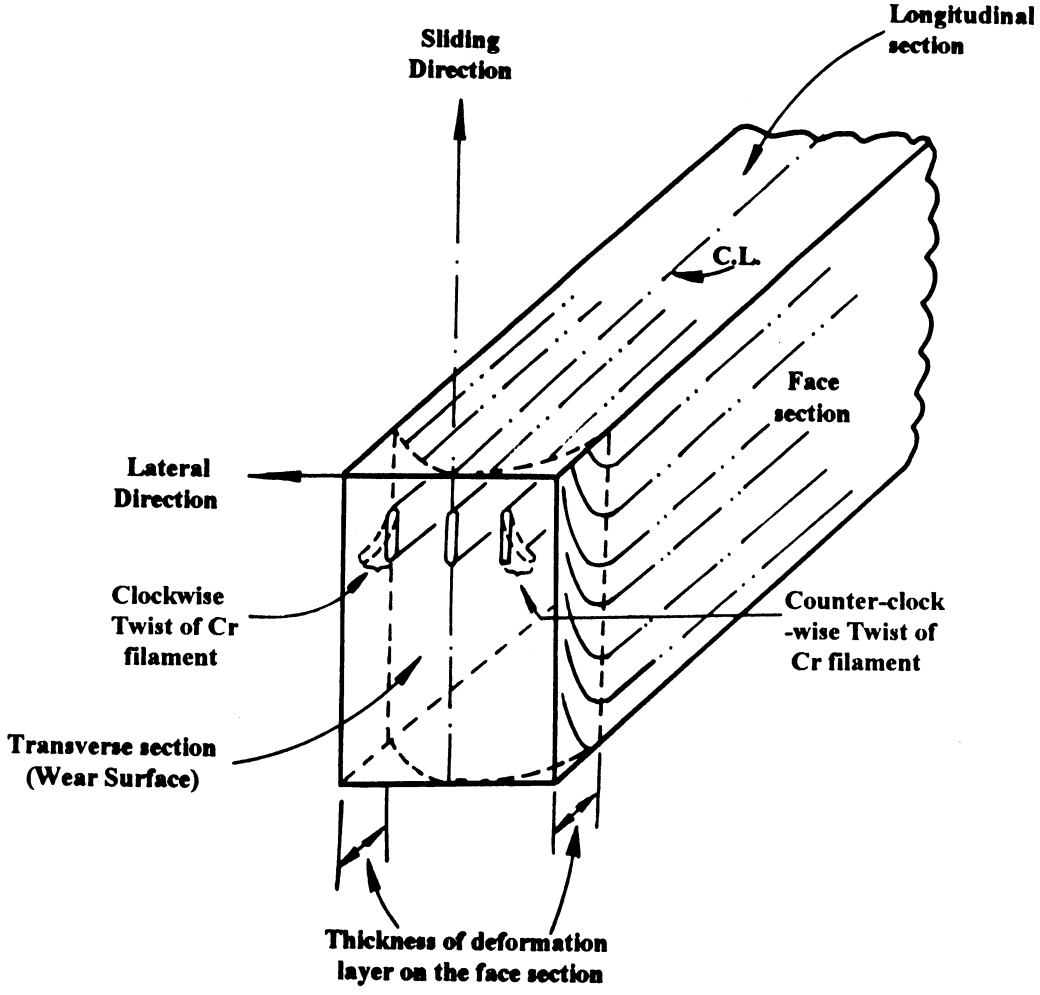

Figure 10. Schematic of subsurface plastic deformation pattern of the Cu-15vol.%Cr composite due to sliding.

the centerline (C.L.) of the pin, which could be expected from simple contact mechanics since a flat punch had maximum stresses at the edges. Figure 11 shows the face section microstructure of the composite below the worn surface after sliding under a normal pressure of 0.06 or 0.44 MPa and at a speed of 3.70 m s^{-1}. No debonding occurred between the Cu matrix and the Cr filaments. The sliding-induced plastic deformation layer was revealed by the change in alignment of the Cr filaments. Under a lower normal pressure, most of the Cr filaments were bent in the sliding direction, as shown in Fig. 11(a). Under a higher normal pressure, however, Cr filament refinement was seen as a major characteristic (Fig. 11 (b)).

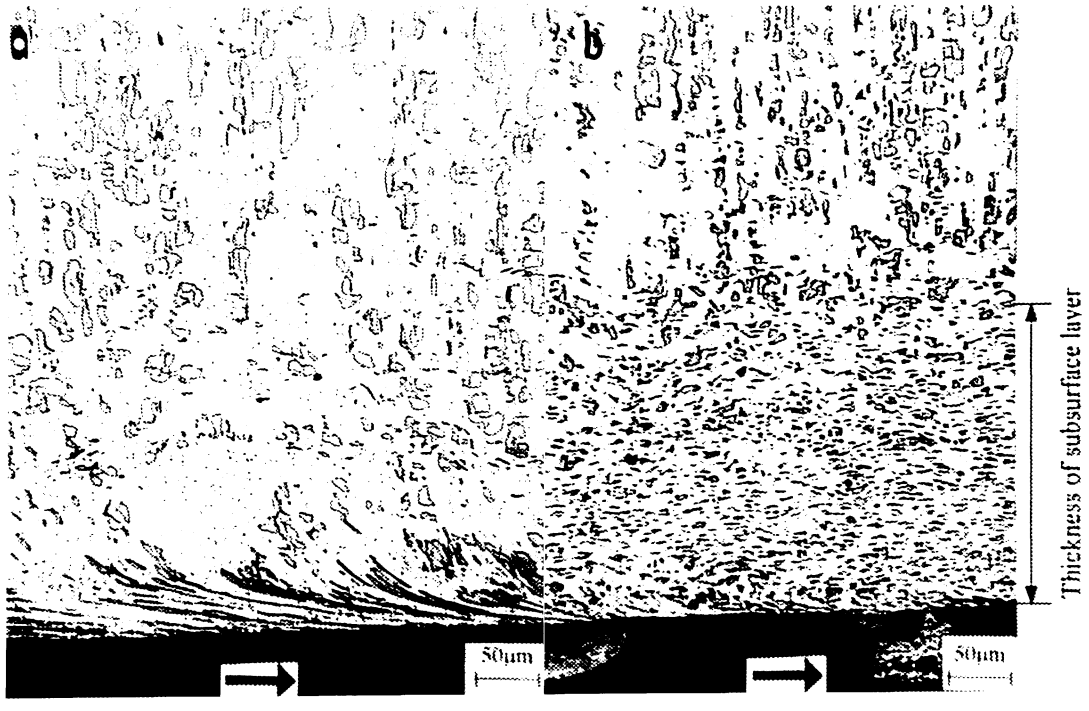

Figure 11. Microstructural change of the Cu-15vol.%Cr *in situ* composite pin after sliding against a hardened AISI 52100 disk at a speed of 3.70 m s^{-1} for 60 min under dry non-electrical sliding. (a)under a normal pressure of 0.06 MPa; (b) under a normal pressure of 0.44 MPa. The arrow indicates the sliding direction.

In addition to producing a flow in the sliding direction within the deformation layer, the sliding force also produced a flow in the lateral directions defined on Fig. 10. This flow was revealed by twisting of the filaments demonstrated in Fig. 12. Figure 12(a) was taken on the face section and Fig. 12 (b) on the longitudinal section. The sliding direction in Fig. 12 (a) was from the left to the right, as shown by the arrow, whereas the sliding direction in Fig. 12 (b) was from the page toward the reader. The two micrographs in Fig. 12 were matched along the edge located at the upper left corner of Fig. 10. The magnification is so high that only the sliding affected layer appears in the micrographs, and that Fig. 12 (a) corresponds to the lower portion of Fig. 11 (b). Figure 12 (b) illustrates the twisting action produced by the flow in the lateral direction. As shown in Fig. 10 the lateral flow produced a twisting action in opposite directions on

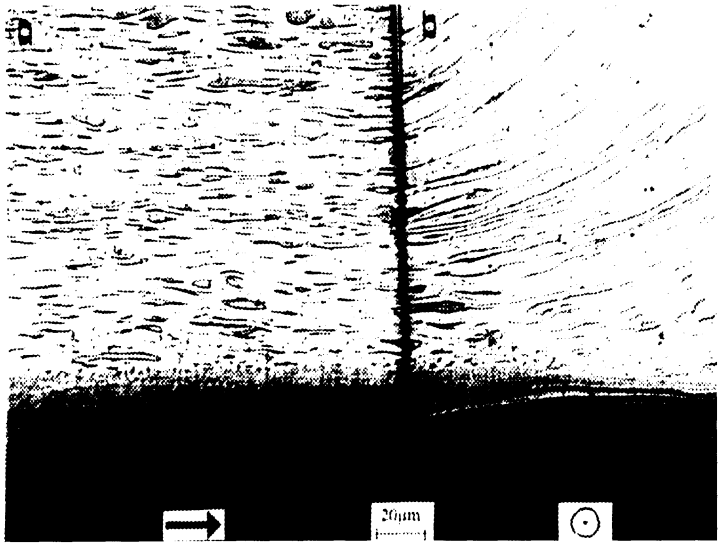

Figure 12. Matched micrographs of the Cu-15vol.%Cr *in situ* composite pin, after dry non-electrical sliding for 60 min at a speed of 3.7 m s^{-1} and under a normal pressure of 0.31 MPa. (a) face section; (b) longitudinal section. The arrow indicates the sliding direction.

the two sides of the rectangularly shaped pin, a clockwise rotation near the left face and a counter clockwise rotation near the right face. Figure 13 presents a model of the shape change involved in Cr filaments. The filaments were elongated along the sliding direction while they were twisted in the lateral directions.

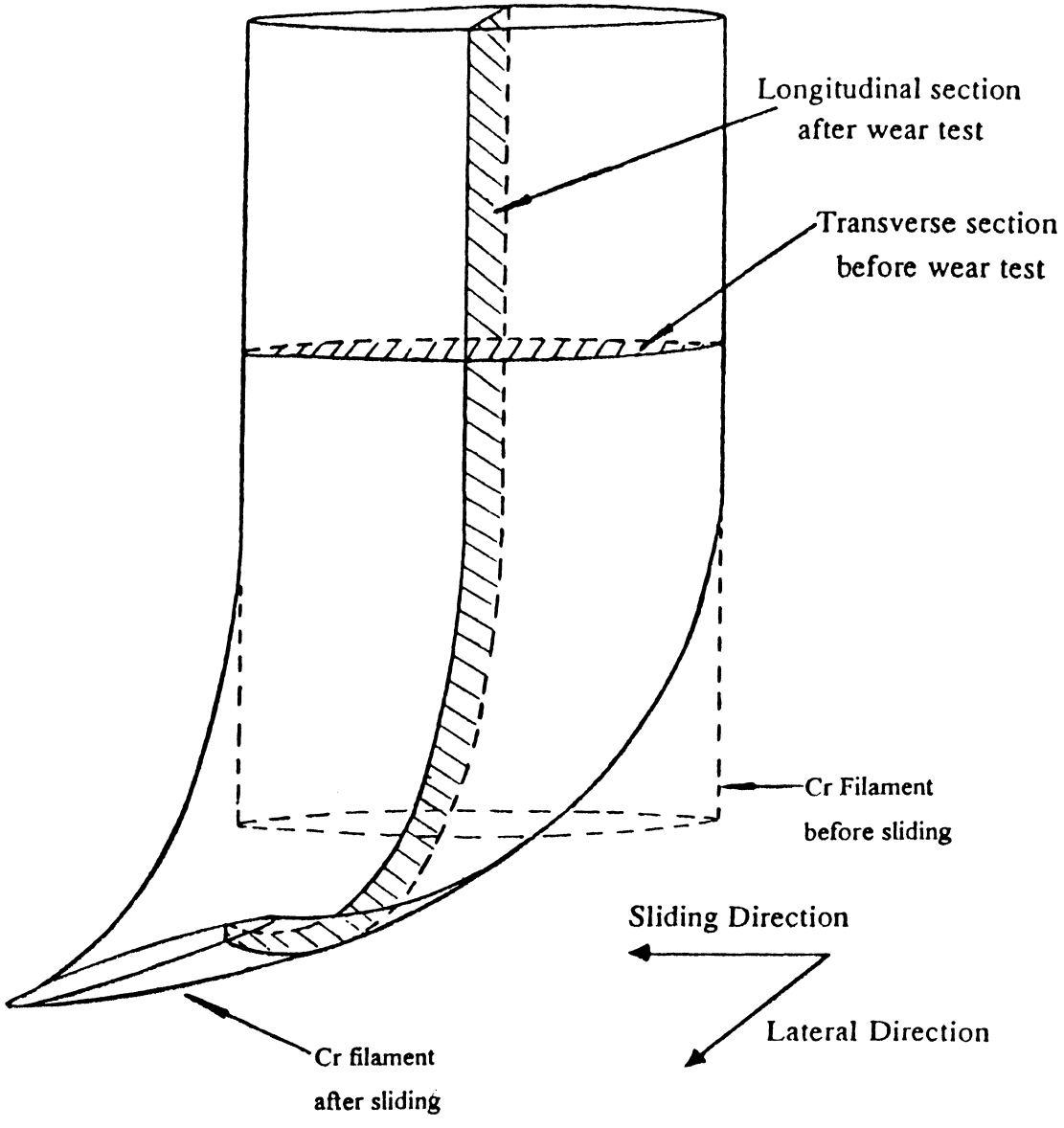

Figure 13. Schematic model of spatial shape change in the ribbon-like Cr filament during sliding wear process.

4.1.4 Thickness of Subsurface Layer

The thickness of the subsurface deformation layer was defined as the distance from the zone of unchanged microstructure to the worn surface on the face section, as shown in Fig 11(b). Figure 14 shows the variation of the thickness of the subsurface deformation layer with normal pressure for the composite slid at a speed of 3.7 m s^{-1}. The thickness data were an average over 18 equally-spaced measurements along the entire contact length of the pin in the sliding direction. It is noted that the thickness increased from 52 μm to 246 μm, when normal pressure increased from 0.06 to 0.44 MPa.

The variation of the thickness of the subsurface deformation layer with sliding speed for the composite slid under a normal pressure of 0.31 MPa is shown in Fig. 15. The thickness of the subsurface deformation layer increased linearly with sliding speed. At a sliding speed of 2.78 m s^{-1}, the thickness of the subsurface deformation layer was 159 μm, and at a sliding speed of 5.56 m s^{-1}, the thickness was 309 μm.

According to Figs. 14 and 15, it can be seen that both increased pressure and sliding speed increased the thickness of the subsurface deformation layer. The subsurface deformation layer was caused by shear stress due to friction when the composite pin slid against the hardened steel disk. Increasing normal pressure would cause more asperities of the composite to contact with those of the disk and therefore increase the friction force. This increased the asperity stress that caused a larger extent of plastic deformation.

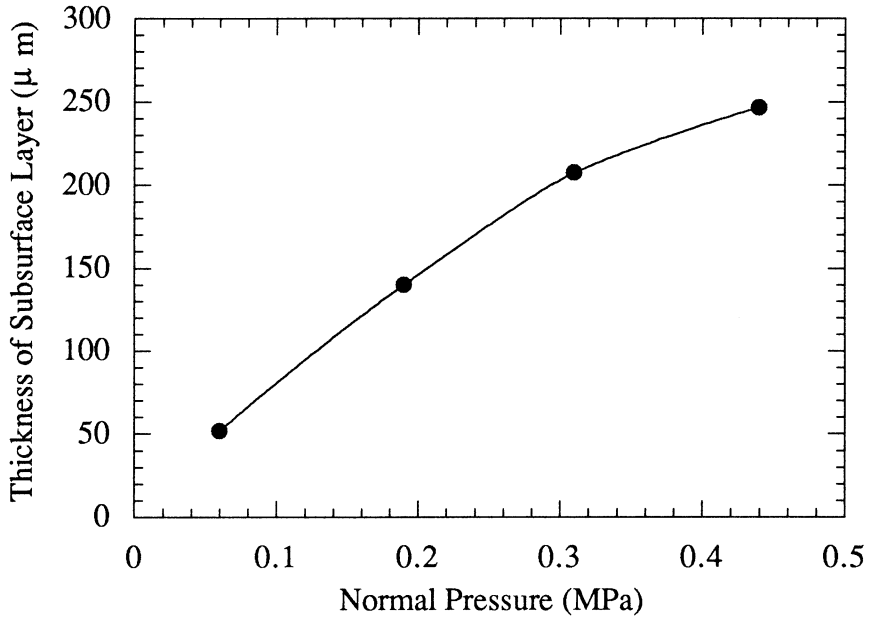

Figure 14. Variation of thickness of subsurface deformation layer with normal pressure at a sliding speed of 3.7 m s^{-1} under dry non-electrical sliding.

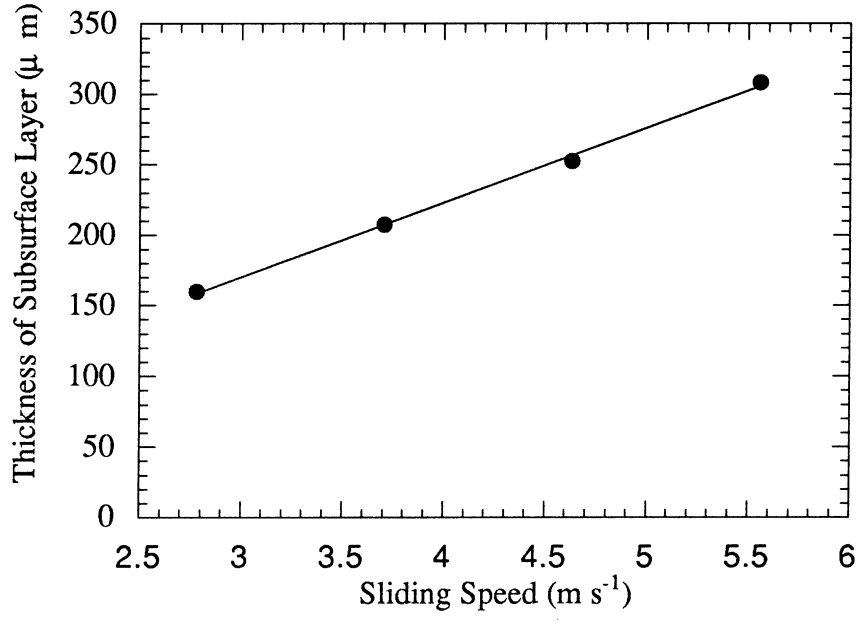

Figure 15. Variation of thickness of subsurface deformation layer with sliding speed under a normal pressure of 0.31 MPa for dry non-electrical sliding.

4.1.5 Wear Mechanism of Non-Electrical Sliding

The Cr filaments demonstrated good strain compatibility with the Cu matrix during the fabrication of the composite. It is not surprising, therefore, that the composite displayed a good strain compatibility between its constituents during sliding and that no debonding was observed between the Cr filaments and the Cu matrix. This sliding-induced deformation found in the Cu-Cr system was similar to that found in the Cu-Nb system (Chen, Liu, Verhoeven & Gibson, 1995).

The slip mechanism of the lateral twist can be explained with the favored crystal slip systems depicted in Fig. 16. Since the ribbon-like Cr filaments were embedded in the softer Cu matrix, plastic deformation of the Cu-15vol.%Cr *in situ* composite was controlled by the deformation mode of the harder Cr filaments. According to Hardwick *et al.* (1991), a texture was developed in the Cr filaments because of the heavy deformation processing. The main rolling texture for the body-centered cubic Cr could be identified as (001)[110]. The (110) crystal plane of the Cr filaments lay in the sliding surface, and the crystal directions $[1\bar{1}1]$ and $[\bar{1}\bar{1}1]$ were 45° with the sliding direction. Therefore, both $(110)\ [1\bar{1}1]$ and $(110)\ [\bar{1}\bar{1}1]$ slip systems could be easily activated during sliding. Slip motion 45° away from the sliding direction in the Cr filaments could account for both elongation in the sliding direction and twist in the lateral directions.

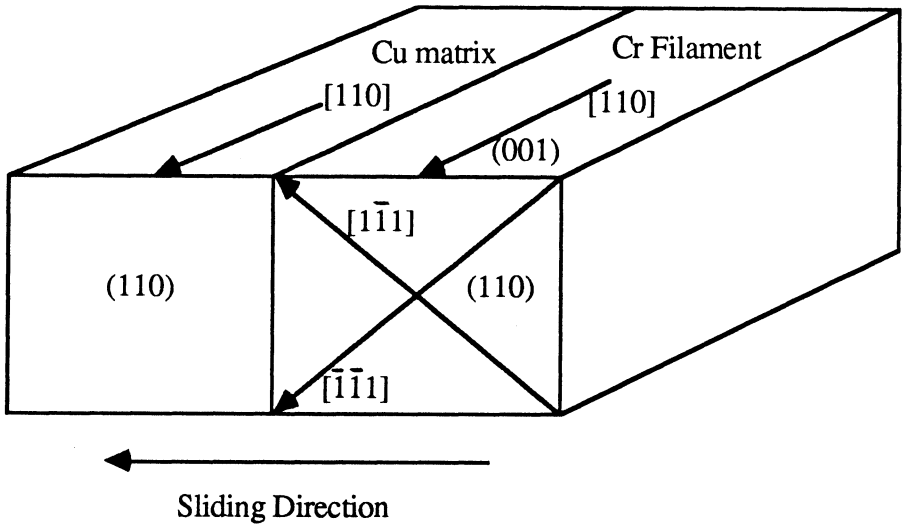

Figure 16. Schematic crystal deformation model for the Cu-15vol.%Cr *in situ* composite.

As illustrated by comparing Fig. 11 (a) with Fig. 11 (b), the subsurface deformation layer was less extensive under a lower normal pressure than under a higher normal pressure. It appears that Fig. 11 (a) showed the beginning of plastic deformation of Cr filaments, while in Fig 11 (b) the plastic deformation of Cr filaments was well developed both in the sliding direction and in the lateral directions. The figures confirm that increasing normal pressure causes more plastic deformation in the contact subsurface region. The SEM micrograph of the worn surface shown in Fig. 17 also reveals the plastic deformation flow on the worn surface. This surface deformation flow was affected by wear debris and transferred material. Figure 18 shows a micrograph of the composite microstructure located just below the worn surface. The specimen was

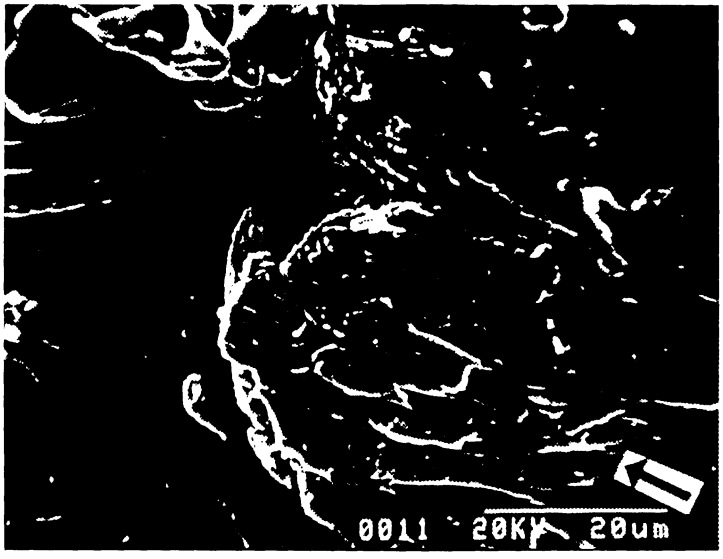

Figure 17. SEM micrograph revealed plastic deformation flow, after dry non-electrical sliding for 30 min at a speed of 3.7 m s^{-1} and under a normal pressure of 0.31 MPa. The arrow indicates the sliding direction.

sectioned slightly below but parallel to the worn surface. The central black region indicates the presence of a wear debris, back-transferred material and oxide, on the surface. The orientation of the Cr filaments clearly shows that the surface deformation flow was affected by the transferred material.

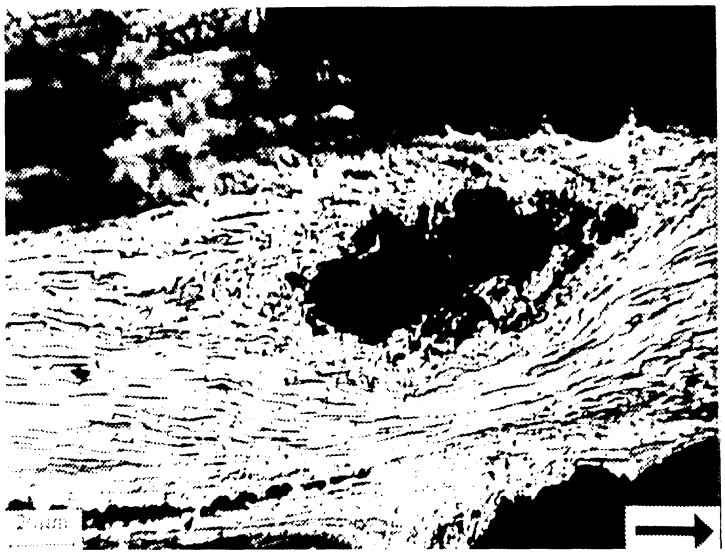

Figure 18. Embedded wear debris inhibited the plastic deformation flow. The arrow indicates the sliding direction.

The complex flow pattern in the deformation layer revealed by the change in orientation of the Cr filaments is quite interesting. According to contact mechanics, apparently flow in the direction of the applied force on the worn surface is a maximum at the faces of the pin and decreases to a minimum at the center of the pin. Because the broad faces of the Cr filaments are aligned parallel to the pin faces the bending moment inertia of the filaments in the applied force direction is much higher than it would be perpendicular to this direction. It seems likely, therefore, that the twisting of the filaments occurs because bending in the lateral directions requires a very low stress. Therefore, one would predict that the wear resistance of the composite would be better for sliding directions parallel to the faces of the composite, as studied here, compared to

the orthogonal lateral direction.

During sliding, material transfer was an important factor that affected the dry sliding behavior of the studied tribosystem. Figure 19 shows the original disk surface morphology and the composite transfer films on the disk after sliding at a sliding speed of 3.7 m s^{-1} and under a normal pressure of 0.06 MPa for 60 min. In the orientation where the sliding direction was normal to the ground grooves of the disk, the grooves were covered by the composite transfer film. In the orientation where the sliding direction was parallel to the ground grooves, the transferred film was a little thinner. The ground groves on the steel disk were filled with transferred material and smoothed by the sliding action.

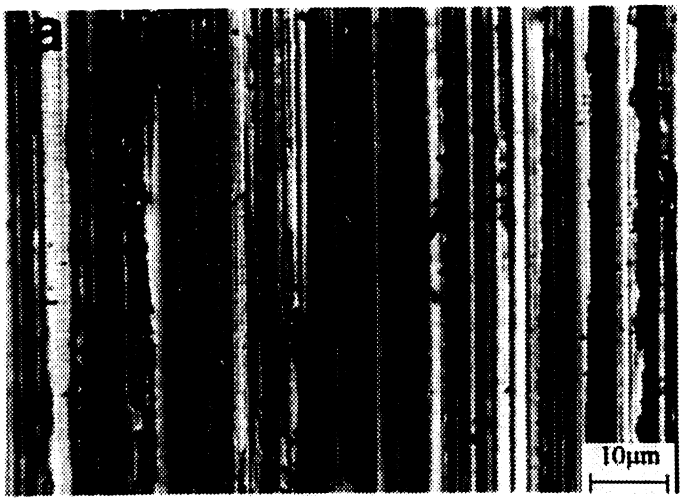

Figure 19. Transfer films on the steel disk for dry non-electrical sliding. (a) the original disk surface; (b) sliding direction normal to the ground groves and (c) sliding direction parallel to the ground groves of the steel disk, sliding at 3.70 m s^{-1} under a normal pressure of 0.06 MPa. The arrow indicates the sliding direction.

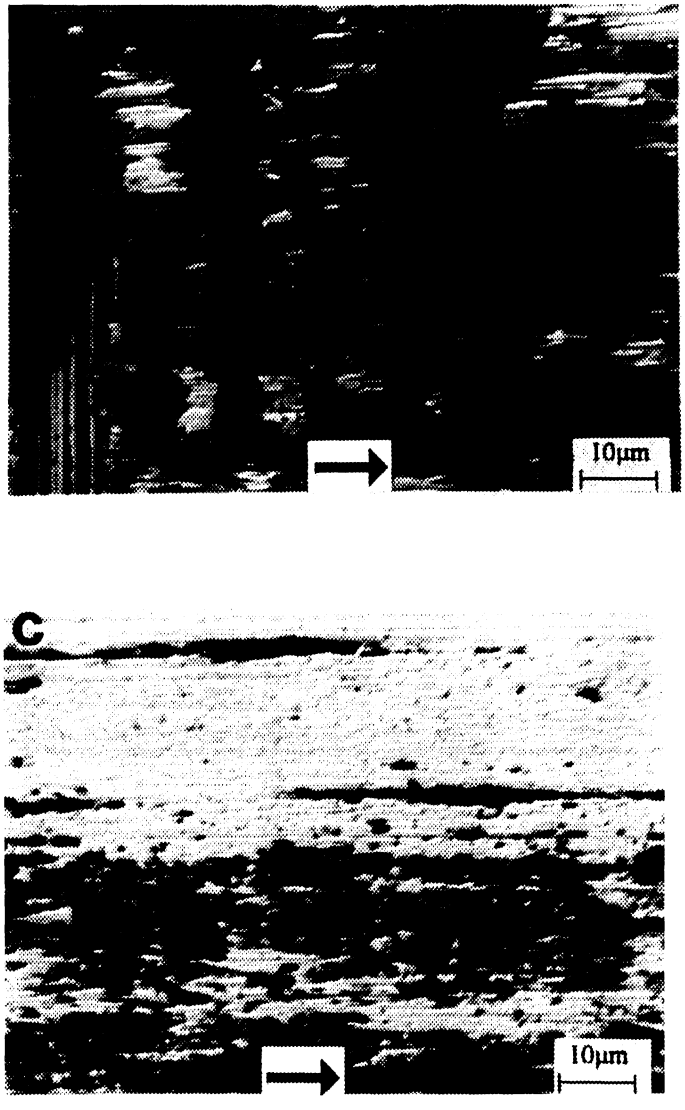

Figure 19. (Continued)

4.2 Dry Electrical Sliding of Cu-15vol.%Cr (Mode II)

4.2 1 Effect of Electrical Current on Coefficient of Friction

The effect of electrical current on average coefficient of friction under three combinations of normal pressure and sliding speed is shown in Fig. 20. The average coefficient of friction decreased significantly with increasing electrical current for all three conditions. For example, the coefficient of friction decreased from 0.99 without electricity to 0.49 with an electrical current of 50 A under a normal pressure of 0.19 MPa and at a sliding speed of 3.33 m s^{-1}. The difference in the coefficient of friction among three test conditions was marginal.

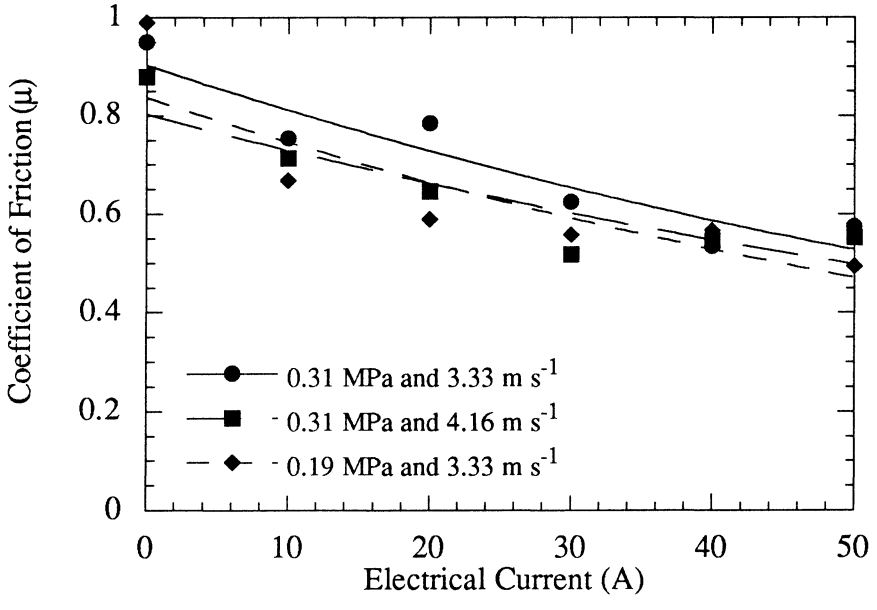

Figure 20. Variation of average coefficient of friction with electrical current for the Cu-15vol.%Cr under dry electrical sliding.

4.2.2 Effects of Electrical Current on Bulk Temperature

Figure 21 shows the variation of average bulk temperature of the Cu-15vol.%Cr pin with electrical current. The tests were performed under a normal pressure of 0.31 MPa and at a sliding speed of 4.16 m s^{-1}. It is noted that the temperature increased slowly under a lower electrical current and increased rapidly in the middle regime of electrical current. A maximum temperature of 120 °C was reached with an electrical current of 50 A. It was observed that Joule heating by electrical current and arcing made a significant contribution to the bulk temperature at higher electrical currents.

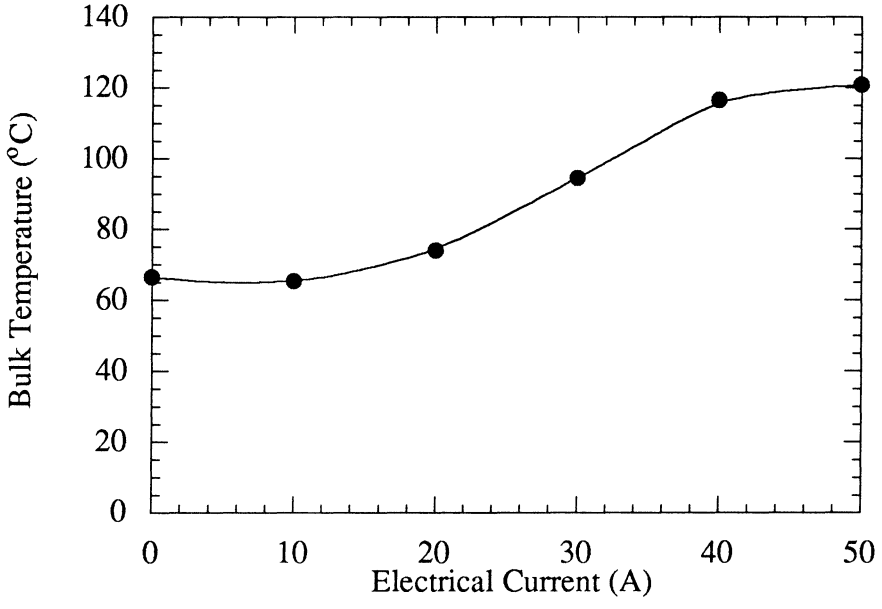

Figure 21. Variation of average bulk temperature with electrical current for the Cu-15vol.%Cr under dry electrical sliding.

At lower electrical currents, both friction and Joule heating contributed to the bulk temperature rise. For example, the average coefficient of friction decreased from 0.88 at 0 A to 0.71 at 10 A as in Fig. 20. The decrease in the coefficient of friction led to a 3.4 W reduction in frictional heat. On the other hand, it was observed that the electrical power consumed at the specimen was about 4 W when a nominal electrical current of 10 A was applied. Thus, frictional heat decrease and electrical Joule heat increase played a nearly equal opposite role in increasing the bulk temperature. This explained the fact that the temperature increased only slightly with increasing current at low currents.

4.2.3 Effect of Electrical Current on Wear

Figure 22 shows the variation of wear rate with electrical current under two normal pressures and two sliding speeds. It is noted that the wear rate of Cu-15vol.%Cr decreased with increasing electrical current. The wear rate under a normal pressure of 0.31 MPa and at a sliding speed of 4.16 m s^{-1} showed a steady decreasing trend with increasing electrical current and was lowest among three test conditions. At the highest current of 50 A, the wear rate reached a minimum for all three test conditions. The wear rate at 50 A was approximately ten times lower than that without electricity.

The difference in the wear rate was larger under a lower electrical current than under a higher current. This difference caused by different tribological parameters became smaller when the electrical current increased. In other words, effects of normal pressure and sliding speed on the wear rate dominated at a lower electrical current level. However, at a higher electrical current, effects of normal pressure and sliding speed on

the wear rate were overwhelmed by that of electrical current.

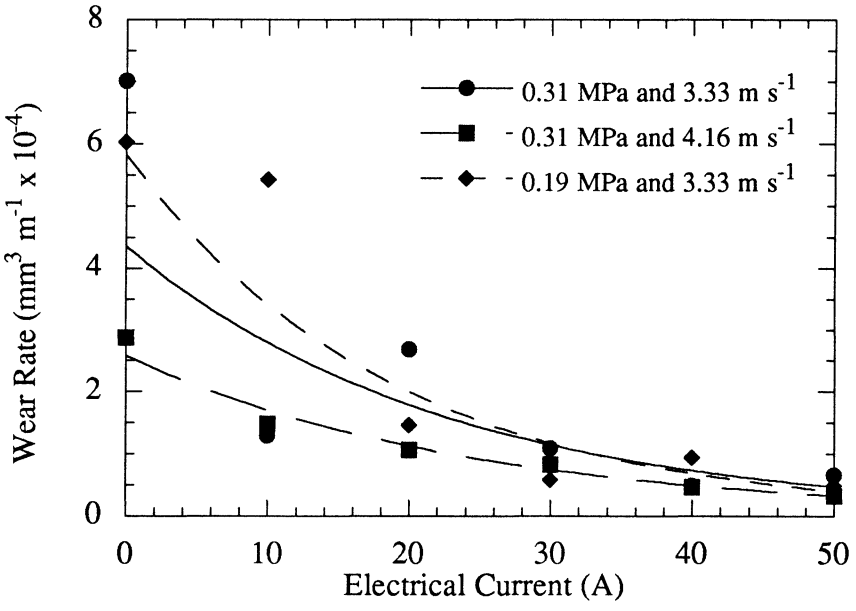

Figure 22. Variation of wear rate with electrical current for the Cu-15vol.%Cr slid under dry conditions.

4.3 Lubricated Electrical Sliding of Cu-15vol.%Cr (Mode III)

4.3.1 Coefficient of Friction

Figure 23 shows the variation in coefficient of friction with normal pressure at a sliding speed of 3.87 m s^{-1} and under electrical currents of 10 and 50 A. Under an electrical current of 50 A, the coefficient of friction significantly decreased with increasing normal pressure. Under an electrical current of 10 A, however, the coefficient of friction slightly decreased with increasing normal pressure. The coefficient of friction under an electrical current of 50 A was always higher than that under an electrical current of 10 A. This behavior is opposite to dry electrical sliding as discussed in 4.2.1 in which the coefficient of friction decreased with increasing electrical current. It is noted that the coefficient of friction under lubricated conditions was less than 0.24. Compared with the coefficient of friction under dry electrical sliding, lubricating oil could significantly reduce the coefficient of friction from 0.5 to 0.24. With increasing electrical current, lubricating oil was degraded and depleted more quickly due to arcing and temperature rise and therefore the coefficient of friction increased.

Figure 24 shows the variation of coefficient of friction with sliding speed under a normal pressure of 0.62 MPa and an electrical current of 10 and 50 A. The coefficient of friction did not change significantly with increasing sliding speed under both electrical currents. Moreover, the coefficient of friction under an electrical current of 50 A was higher than that under an electrical current of 10 A.

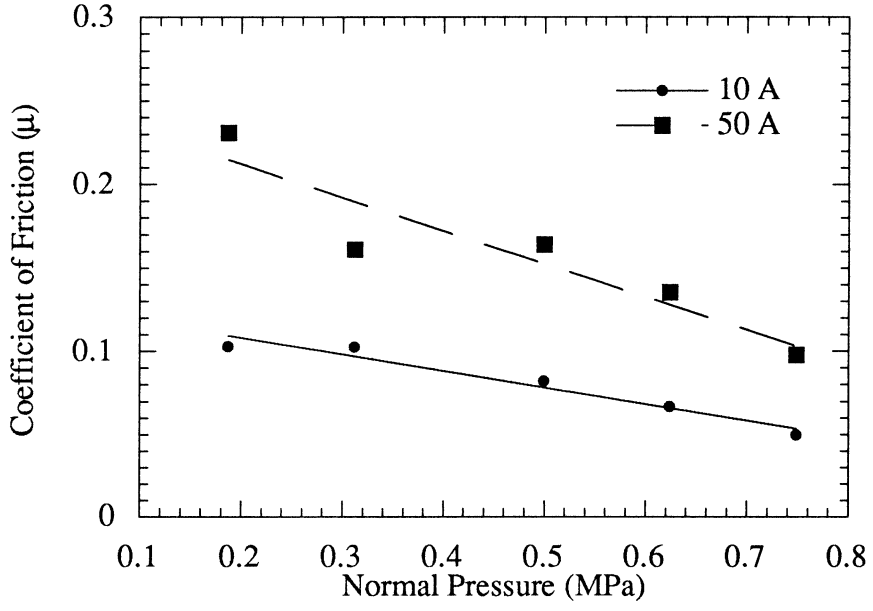

Figure 23. Variation of coefficient of friction with normal pressure for lubricated electrical sliding at a speed of 3.87 m s^{-1}.

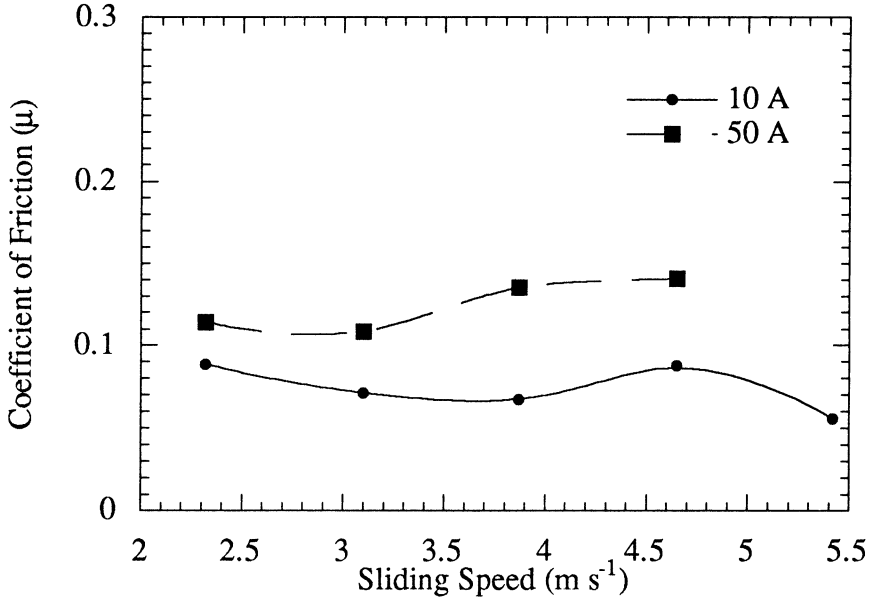

Figure 24. Variation of coefficient of friction with sliding speed for lubricated electrical sliding under a normal pressure of 0.62 MPa.

Figure 25 shows the variation of coefficient of friction with electrical current under a normal pressure of 0.62 MPa and at a sliding speed of 2.32 and 3.87 m s^{-1}. The coefficient of friction increased with increasing electrical current. However, no difference in the coefficient of friction between two sliding speeds could be perceived.

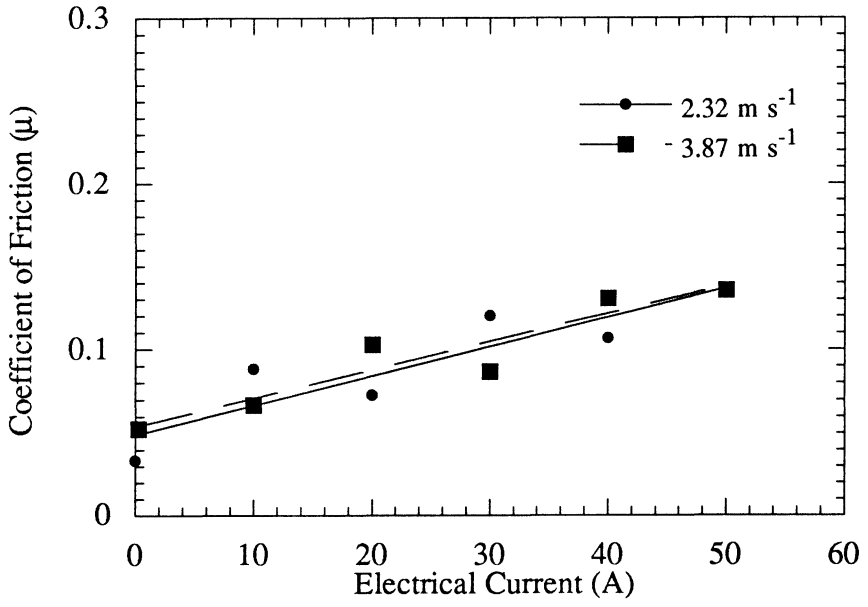

Figure 25. Variation of coefficient of friction with electrical current for lubricated electrical sliding under a normal pressure of 0.62 MPa.

4.3.2 Contact Behavior

4.3.2.1 Static contact resistance

Static contact resistance was first studied as a function of normal pressure under two electrical currents, *i.e.*, 10 and 50 A and under dry and lubricated conditions. Figure 26 shows the variation of static contact resistance with normal pressure. The static contact resistance decreased slightly with increasing normal pressure due to the improved contact. The static contact resistance under an electrical current of 10 A was

approximately twice as large as that under an electrical current of 50 A. On the other hand, the static contact resistance with lubricant was a little lower than that without oil under the same current, except the point tested under a normal pressure of 0.19 MPa and an electrical current of 10 A with oil.

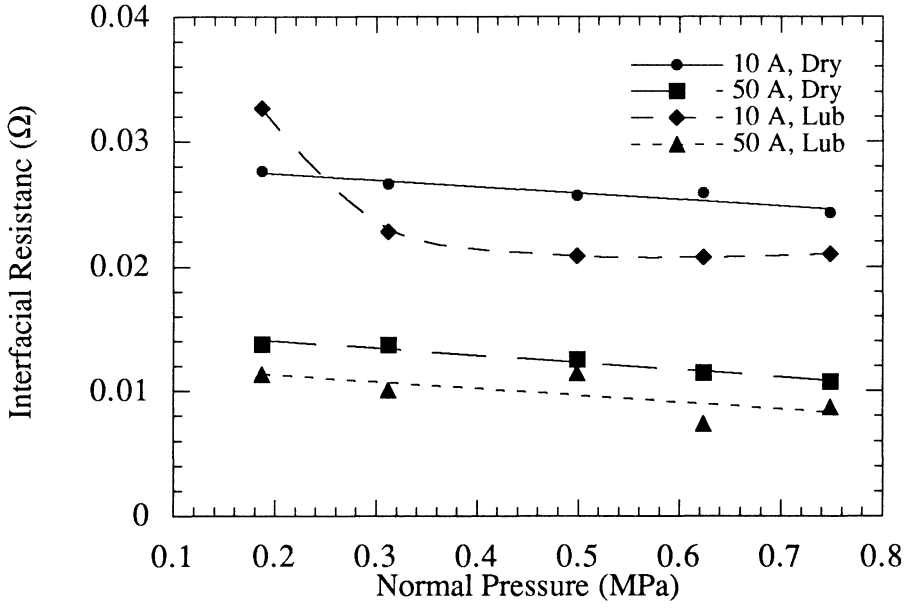

Figure 26. Variation of static interfacial resistance with normal pressure for dry and lubricated conditions.

4.3.2.2 Dynamic contact resistance

The effect of normal pressure on contact resistance at a sliding speed of 3.87 m s^{-1} and under electrical currents of 10 and 50 A is shown in Fig. 27. The contact resistance under an electrical current of 10 A was higher than that under an electrical current of 50 A. In both cases, the contact resistance decreased with increasing normal pressure, which is similar to the static contact.

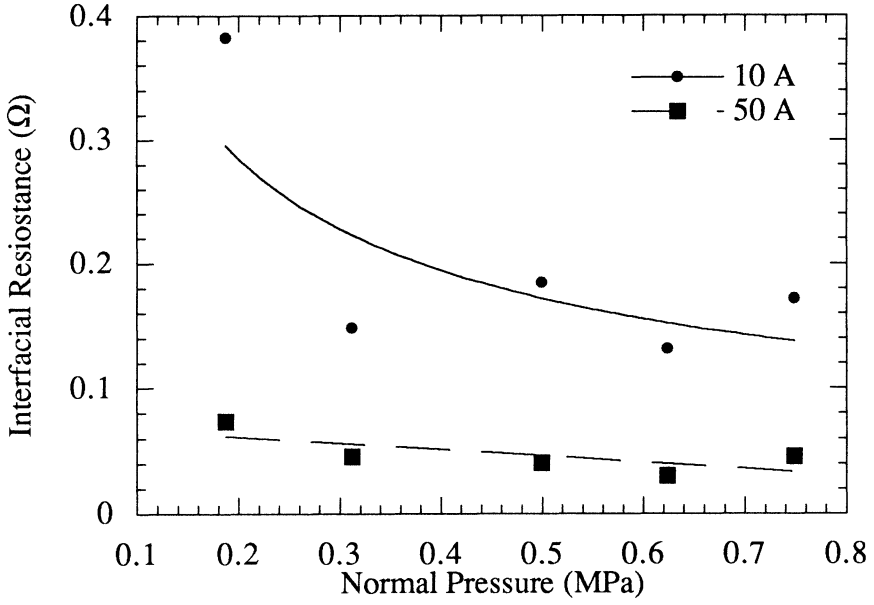

Figure 27. Variation of dynamic interfacial resistance with normal pressure for lubricated electrical sliding at a speed of 3.87 m s^{-1}.

The effect of sliding speed on contact resistance under a normal pressure of 0.62 MPa and electrical currents of 10 and 50 A is shown in Fig. 28. Under an electrical current of 10 A, the contact resistance decreased with increasing sliding speed and was higher than that under an electrical current of 50 A. On the other hand, the contact resistance under an electrical current of 50 A did not significantly change with sliding speed.

Effect of electrical current on contact resistance under a normal pressure of 0.62 MPa and at a sliding speed of 2.32 and 3.87 m s^{-1} is shown in Fig. 29. In both cases, the contact resistance significantly decreased with increasing electrical current. The contact resistance at a higher sliding speed (3.87 m s^{-1}) was consistently lower than that at a lower sliding speed (2.32 m s^{-1}).

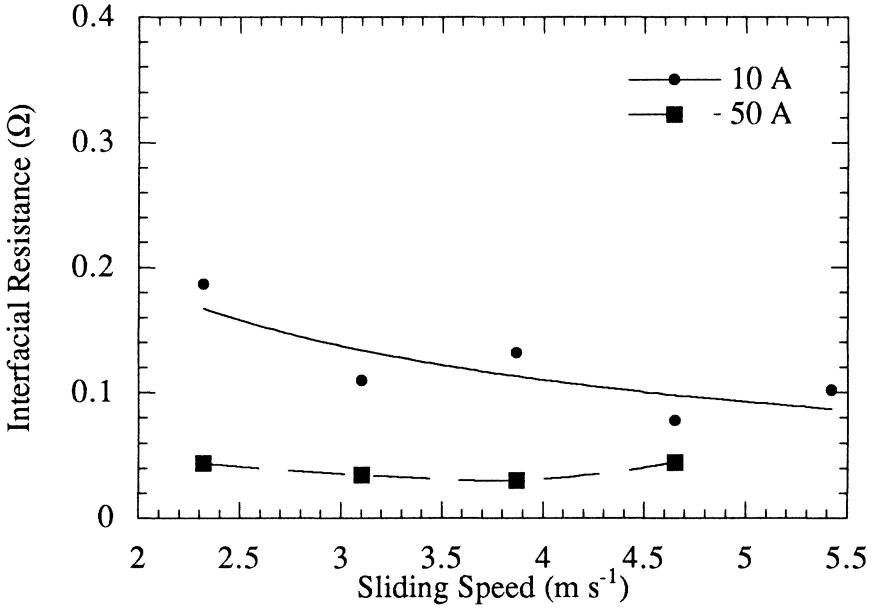

Figure 28. Variation of dynamic interfacial resistance with sliding speed for lubricated electrical sliding under a normal pressure of 0.62 MPa.

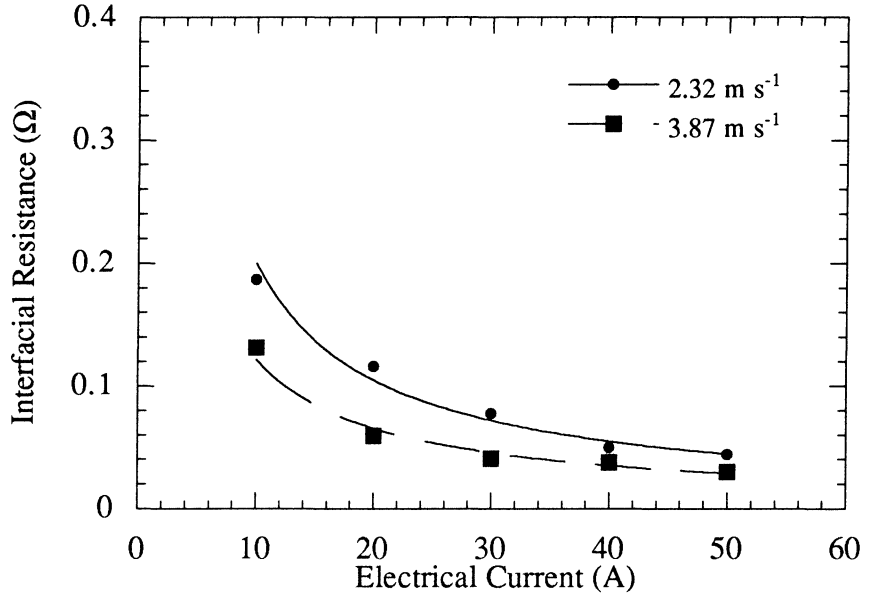

Figure 29. Variation of dynamic interfacial resistance with electrical current for lubricated electrical sliding under a normal pressure of 0.62 MPa.

4.3.2.3 Openness of circuit under sliding

Figure 30 shows the variation of circuit openness with normal pressure for lubricated electrical sliding at a speed of 3.87 m s^{-1}. The openness of circuit decreased rapidly with increasing normal pressure for both electrical currents. When normal pressure increased to 0.30 MPa, the openness of circuit was less than 3%. Further increasing normal pressure resulted in the openness of circuit less than 1%.

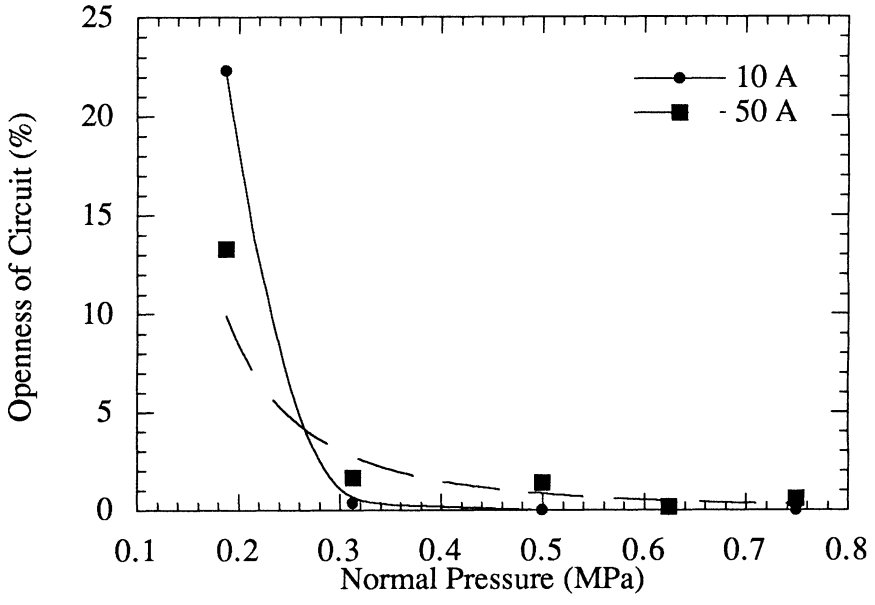

Figure 30. Variation of openness of circuit with normal pressure for lubricated electrical sliding at a speed of 3.87 m s^{-1}.

Figure 31 shows the variation of circuit openness with sliding speed for the lubricated electrical sliding under a normal pressure of 0.62 MPa. The openness of circuit for both electrical currents was less than 1%. The openness of circuit increased with increasing sliding speed.

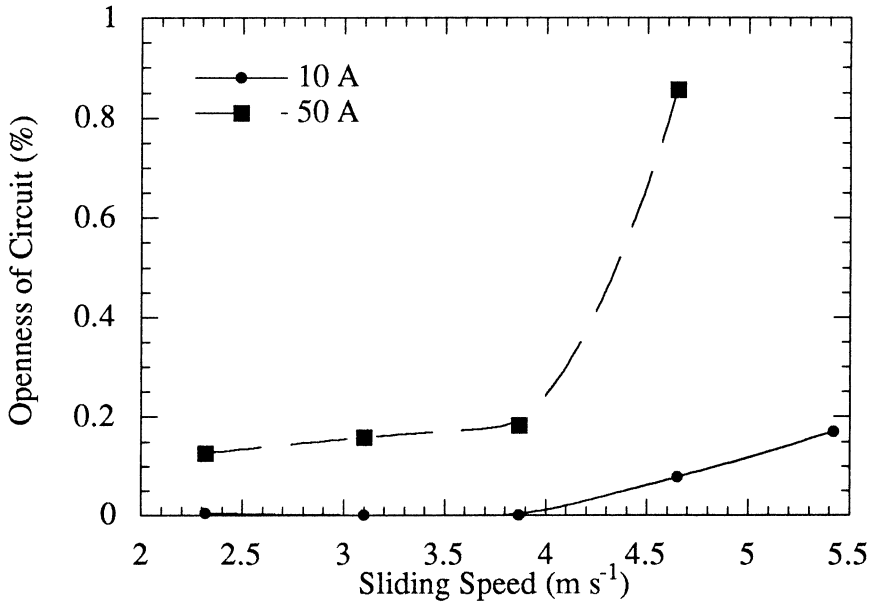

Figure 31. Variation of openness of circuit with sliding speed for lubricated electrical sliding under a normal pressure of 0.62 MPa.

Figure 32 shows the variation of openness of circuit with electrical current for the lubricated electrical sliding under a normal pressure of 0.62 MPa. The openness of circuit increased with increasing electrical current and was less than 1% for both sliding speeds.

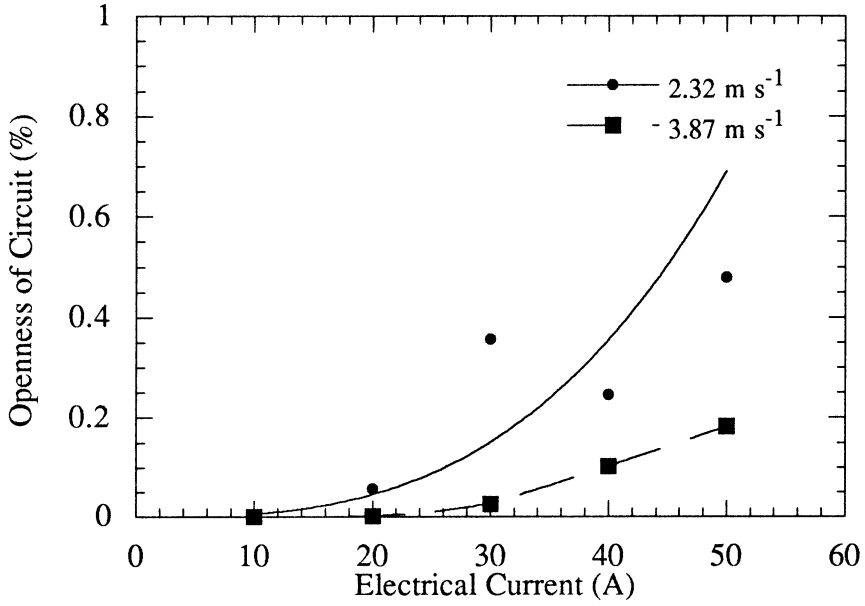

Figure 32. Variation of circuit openness with electrical current for lubricated sliding under a normal pressure of 0.62 MPa.

4.3.3 Bulk Temperature

The variation of bulk temperature with electrical current for lubricated sliding under a normal pressure of 0.62 MPa and at a sliding speed of 2.32 and 3.87 m s^{-1} is shown in Fig. 33. The bulk temperature increased with increasing electrical current for both sliding speeds.

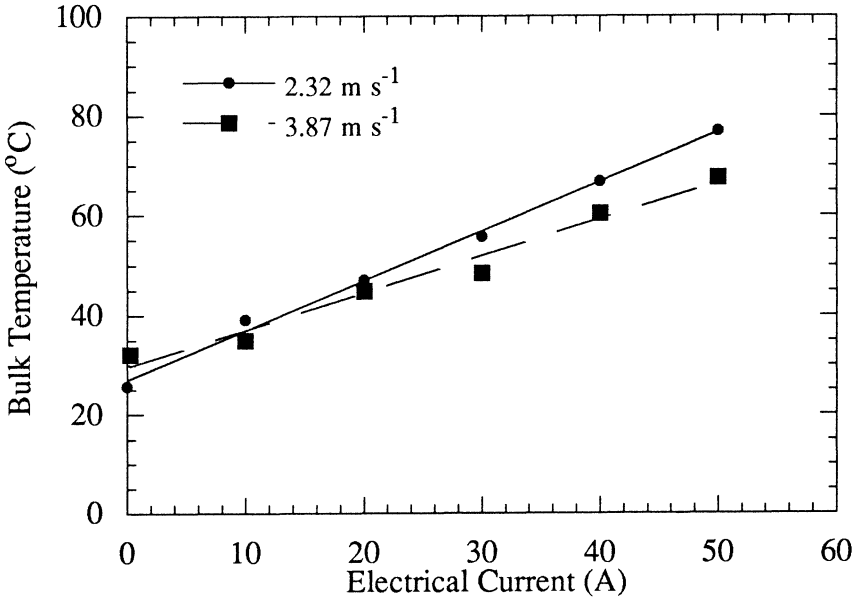

Figure 33. Variation of bulk temperature with electrical current for lubricated sliding under a normal pressure of 0.62 MPa.

As in the dry electrical sliding, the Joule heating was significant in the lubricated electrical sliding. The highest bulk temperature was reached under an electrical current of 50 A for both sliding speeds. Because the coefficient of friction was significantly reduced by lubricant, frictional heating and the shear stress for the subsurface deformation layer decreased. That can partly explain why the bulk temperature under the lubricated electrical sliding was lower than that under the dry electrical sliding.

4.3.4 Wear Rate

The effect of normal pressure on lubricated sliding wear rate at a sliding speed of 3.87 m s^{-1} and under electrical currents of 10 and 50 A is shown in Fig. 34. The wear rate under an electrical current of 50 A was much higher than that under an electrical current

of 10 A. Under an electrical current of 10 A, the wear rate increased slightly with increasing normal pressure. Under an electrical current of 50 A, the wear rate first decreased with increasing normal pressure up to 0.62 MPa and then increased.

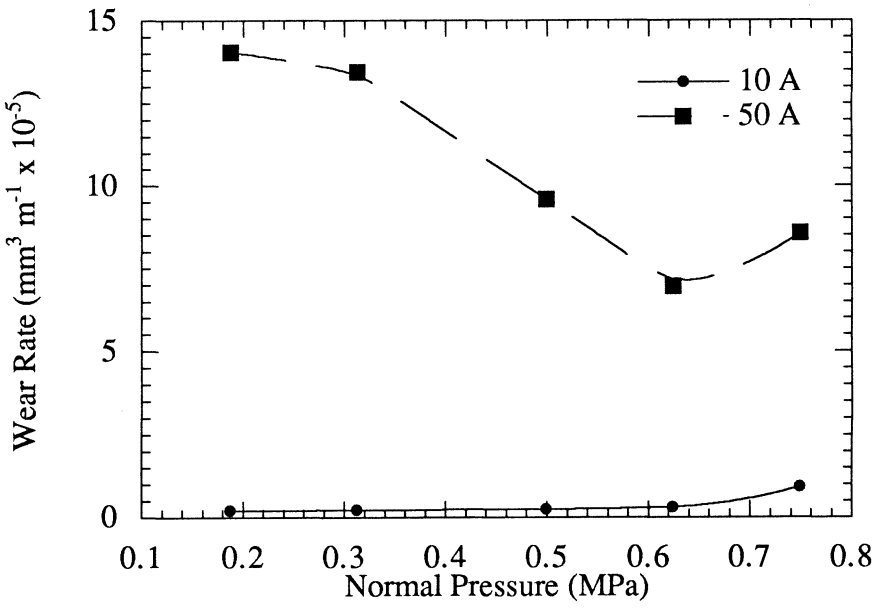

Figure 34. Variation of wear rate with normal pressure for lubricated electrical sliding at a speed of 3.87 m s^{-1}.

The variation of wear rate with sliding speed under a normal pressure of 0.62 MPa and electrical currents of 10 and 50 A is shown in Fig. 35. The wear rate under an electrical current of 50 A was much higher than that under an electrical current of 10 A. Under an electrical current of 10 A, the wear rate decreased with increasing sliding speed, while under an electrical current of 50 A, the wear rate decreased first and then increased.

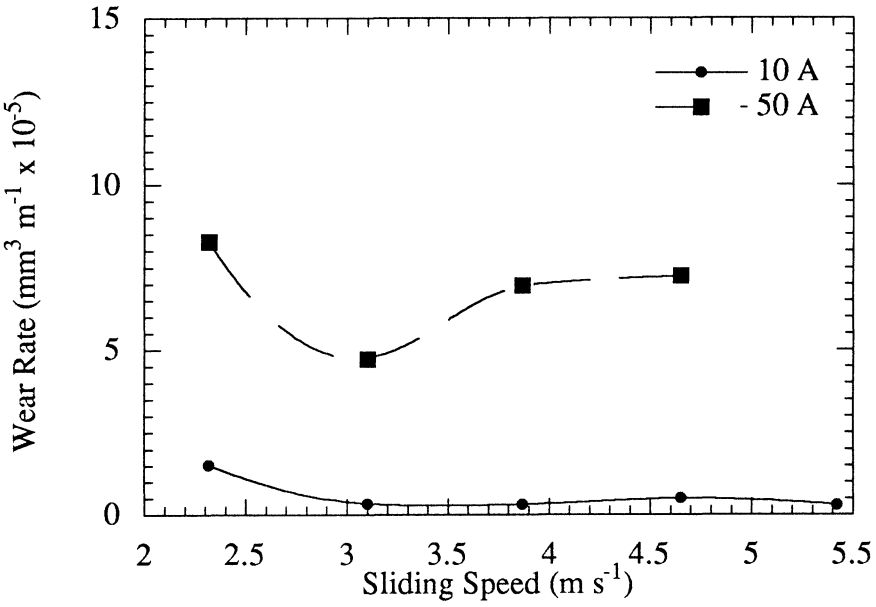

Figure 35. Variation of wear rate with sliding speed for lubricated electrical sliding under a normal pressure of 0.62 MPa.

The effect of electrical current on wear rate for lubricated electrical sliding under a normal pressure of 0.62 and at a sliding speed of 2.32 and 3.87 m s^{-1} is shown in Fig. 36. At both sliding speeds, the wear rate increased with increasing electrical current. Under lower electrical current, the wear rate at a sliding speed of 2.32 m s^{-1} was higher than that at a sliding speed of 3.87 m s^{-1}. However, under higher electrical current, the wear rate at a lower sliding speed was lower than that at a higher sliding speed.

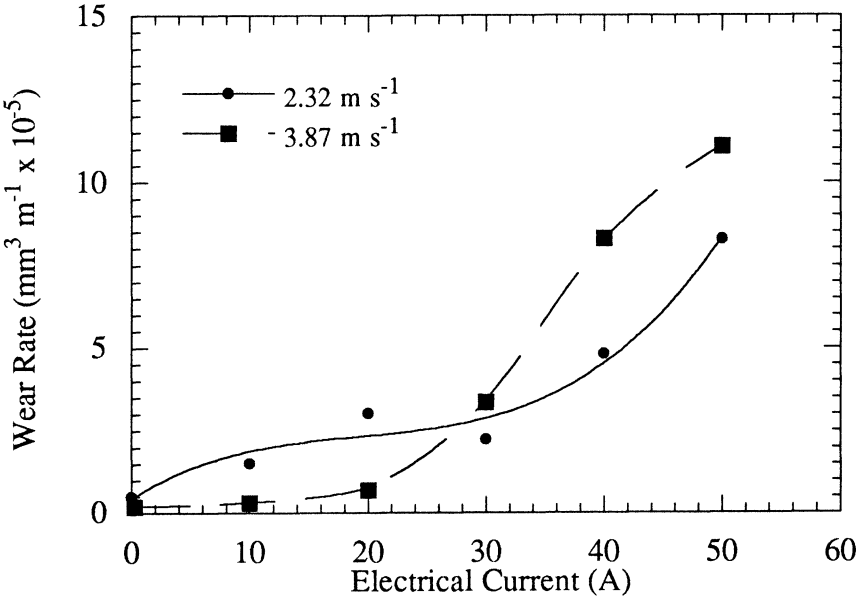

Figure 36. Variation of wear rate with electrical current for lubricated electrical sliding under a normal pressure of 0.62 Mpa.

4.4 Microstructural Change during Electrical Sliding

Because of sliding, the composite pin underwent a change in microstructure near the worn surface, which is similar to that under the dry non-electrical sliding discussed in 4.1.3. Figure 37 (a) shows the microstructural change occurred near the worn surface of the Cu-15vol.%Cr composite pin after the dry electrical sliding for 60 min under a normal pressure of 0.31 MPa, at a speed of 4.16 m s^{-1}, and under an electrical current of 50 A. A three-layer feature, *i.e.*, refined layer, transition layer, and unchanged area, was nearly the same as that for the dry non-electrical sliding. However, a new microstructural feature was introduced, *i.e.*, wear particles produced either by the arc melting or by asperity cutting were trapped in the refined layer and surface film. Figure 37 (b) is an enlarged view of Fig. 37 (a) to show this feature in greater detail. Small spherical

droplets caused by arc melting and wear debris can be observed in the black surface layer.

Figure 37 (c) shows microstructural change occurred near the worn surface after lubricated electrical sliding. The composite pin was tested under a normal pressure of 0.62 MPa, at a sliding speed of 3.87 m s^{-1} and under an electrical current of 50 A. Similar microstructural features, as those observed in the composite tested under dry electrical sliding, were observed. Under the lubricated electrical sliding, however, the refined layer was much thinner than that under the dry electrical sliding. There was not as many trapped wear debris in the refined layer as dry electrical sliding.

Figure 37. Face section microstructure of the Cu-15vol.%Cr *in situ* composite, (a) after dry electrical sliding; (b) enlarged view of interfacial microstructure in (a); (c) after lubricated electrical sliding. Arrow shows sliding direction.

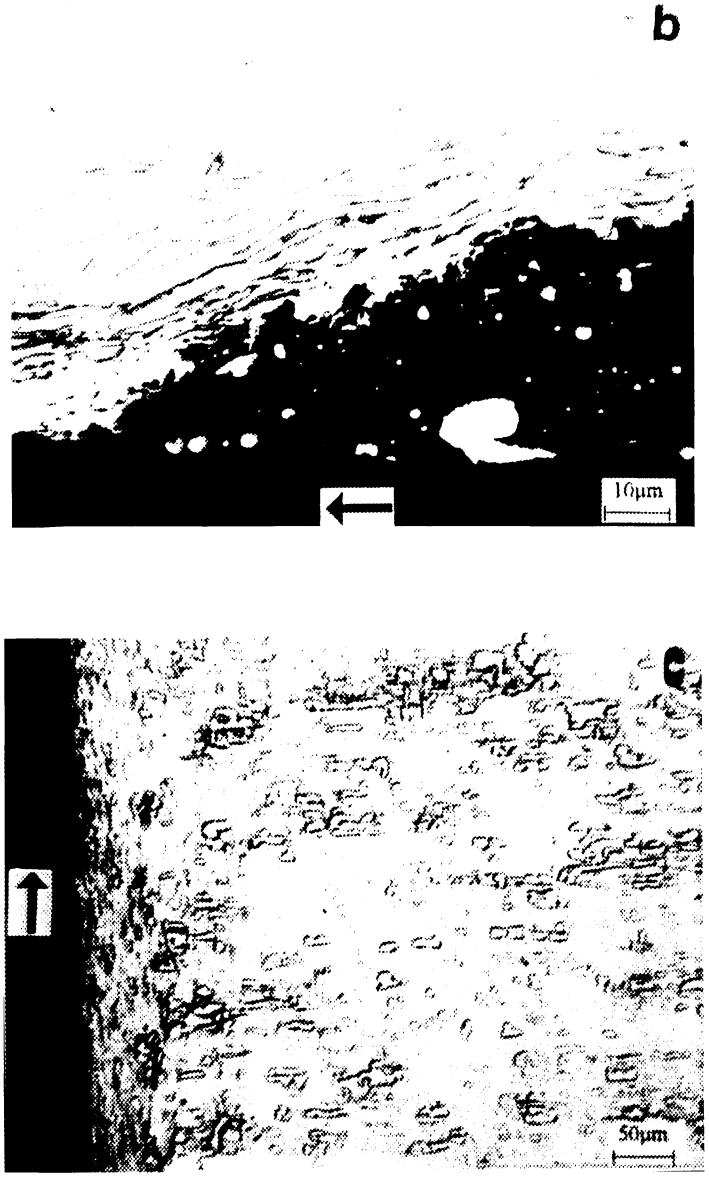

Figure 37. (Continued)

The three-dimensional characteristic of deformed layer and Cr filaments was revealed by SEM micrograph in Fig. 38. The specimen was deeply etched to remove the Cu matrix. There were a layer with fine Cr filaments, filament bent to the sliding direction and twisted, and unchanged Cr filaments. These three features correspond to the refined layer, transition layer and unchanged area, respectively.

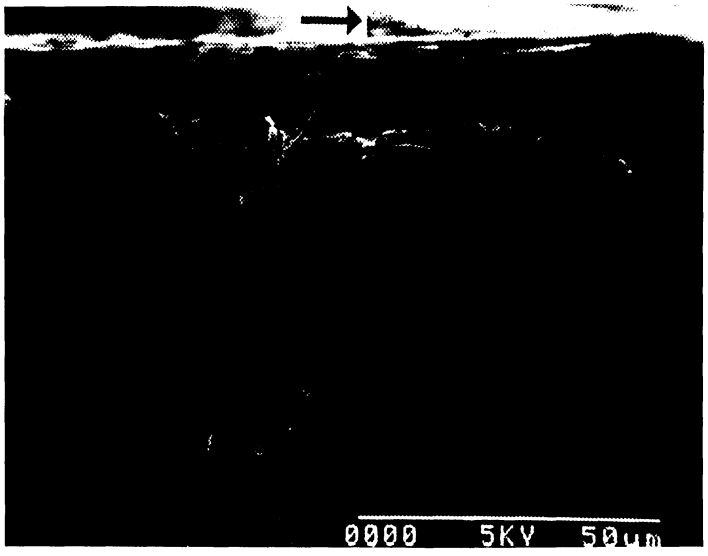

Figure 38. SEM micrograph showed three-layer microstructural feature after lubricated electrical sliding. The Cu matrix was deeply etched. Arrow shows sliding direction.

4.4.1 Effect of Electrical Current on Thickness of Subsurface Layer

The variation of the subsurface deformation layer thickness with electrical current is shown in Fig. 39, for dry and lubricated electrical sliding. Under dry electrical sliding, the thickness initially increased from 117 μm without an electrical load to 125 μm with an electrical current of 10 A before it decreased to 55 μm with an electrical current of 50 A.

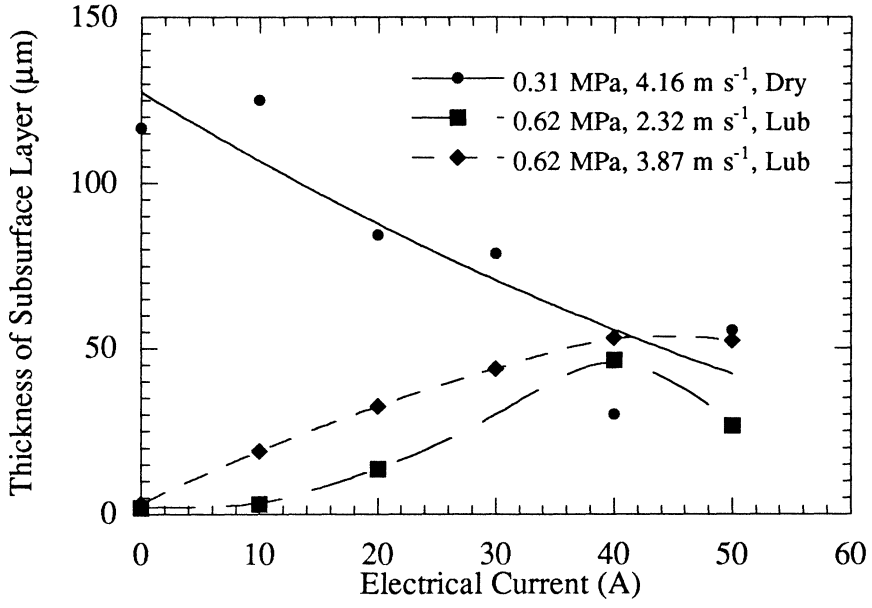

Figure 39. Variation of subsurface deformation layer thickness with electrical current for the Cu-15vol.%Cr under electrical sliding.

Contrary to the dry electrical sliding, the thickness of the subsurface deformation layer increased with increasing electrical current under lubricated sliding. The thickness of the subsurface deformation layer at a sliding speed of 3.87 m s^{-1} was higher than that at a sliding speed of 2.32 m s^{-1}. The main reason for a thicker layer at a higher sliding speed was that lubricant was depleted more quickly. At lower electrical current, the thickness of the subsurface deformation layer for the lubricated electrical sliding was much smaller than for the dry electrical sliding. This could be explained by the fact of a lower coefficient of friction with lubricated sliding. As electrical current increased, the difference in subsurface layer between the lubricated electrical sliding and the dry electrical sliding reduced.

The subsurface layer was caused by plastic deformation due to sliding, which depended on the shear stress due to friction and the yield strength of the Cu-15vol.%Cr composite. The shear stress was proportional to the friction force and the yield strength of the composite was related to temperature. For dry electrical sliding, according to the previous discussion in 4.2.1 and 4.2.2, the friction force (coefficient of friction) decreased with increasing electrical current and the bulk temperature increased with increasing electrical current. Since the pin was softened by increased temperature and arc melting on the surface, the plastic deformation was more limited near the sliding surface. Thus, the thickness of the subsurface deformation layer decreased with increasing electrical current because less shear stress due to friction was applied and the plastic deformation was more concentrated on the softened layer. For lubricated electrical sliding, both the coefficient of friction and the bulk temperature increased with increasing electrical current. Therefore, the thickness of the subsurface deformation layer increased with increasing electrical current.

4.4.2 Effect of Electrical Sliding on Microhardness

The refined layer due to the electrical sliding had different hardness than that of the original Cu-15vol.%Cr for both dry electrical and non-electrical sliding. Figure 40 (a) shows the variation of microhardness with the distance from sliding interface for the Cu-15vol.%Cr slid without an electrical load, under a normal pressure of 0.31 MPa and at a sliding speed of 4.16 m s^{-1}. The microhardness of the composite after dry non-electrical sliding did not change significantly. The highest microhardness was 220 HV.

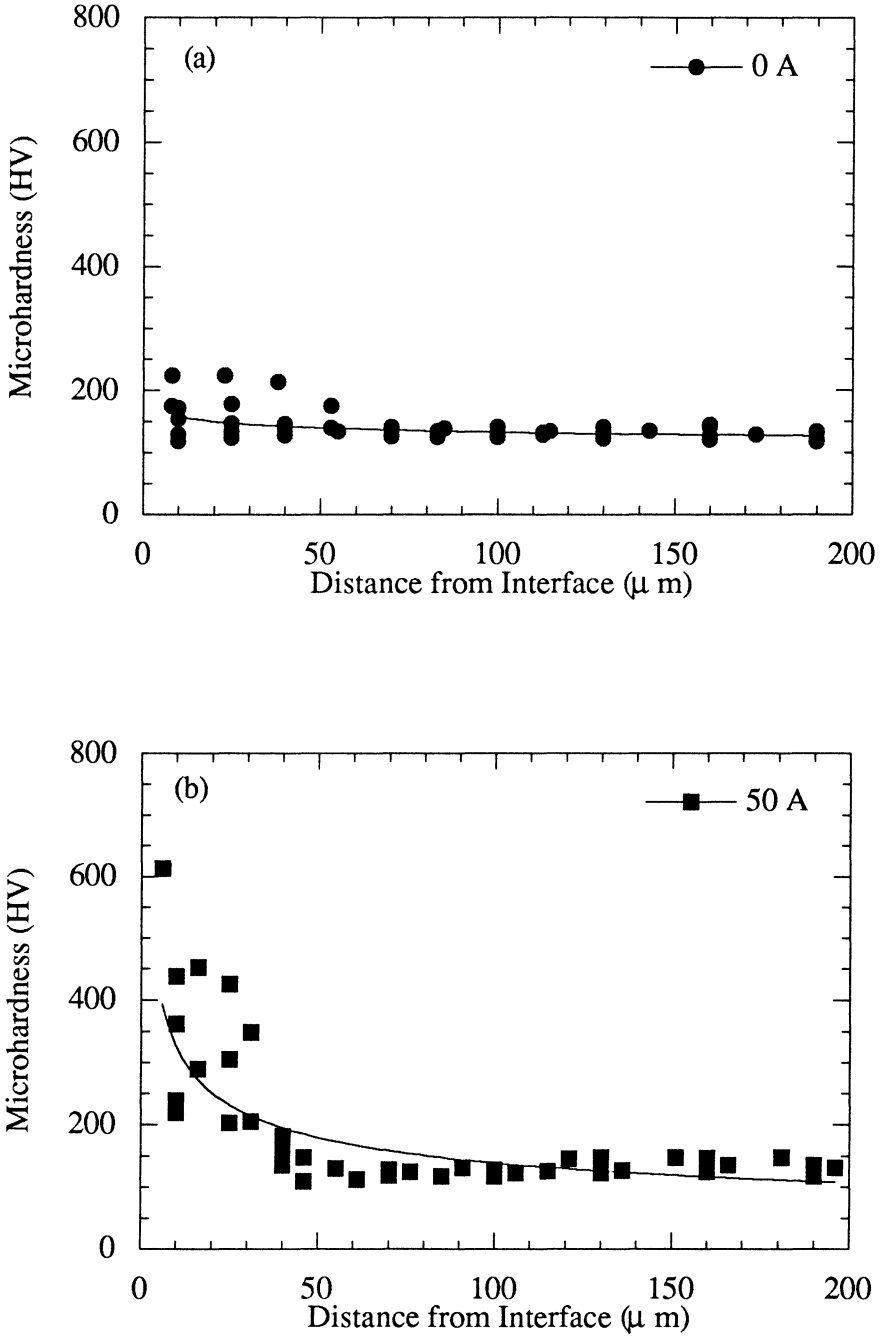

Figure 40. Variation of microhardness for the Cu-15vol.%Cr with the distance from the sliding interface after dry sliding for 60 min under a normal pressure of 0.31 MPa and at a speed of 4.16 m s^{-1}, (a) non-electrical sliding; (b) electrical sliding under a current of 50 A.

Figure 40 (b) is for the composite tested under a normal pressure of 0.31 MPa, at a sliding speed of 4.16 m s^{-1}, and under an electrical current of 50 A. Significantly higher microhardness was measured within an area up to 30 μm from the worn surface. The microhardness decreased rapidly with increasing distance from the sliding surface until it was lowered to that of the bulk material. The higher microhardness obtained from the area close to the worn surface is attributed to a different microstructure caused by the dry electrical sliding. The harder microstructure may be formed by oxidation, localized arc melting, and mechanical alloying of melted Cu-15vol.%Cr with the wear debris and the back transferred materials from the steel disk.

Figure 41 shows the variation of microhardness with the distance from the sliding interface for the lubricated electrical sliding under a normal pressure of 0.62 MPa, at a sliding speed of 3.87 m s^{-1}, and under an electrical current of 50 A. The highest micro-hardness was measured in the refined layer very close to the sliding interface and then hardness was leveled to that of bulk material. The refined layer was thinner under the lubricated electrical sliding and hardness was not as high as that under dry electrical sliding.

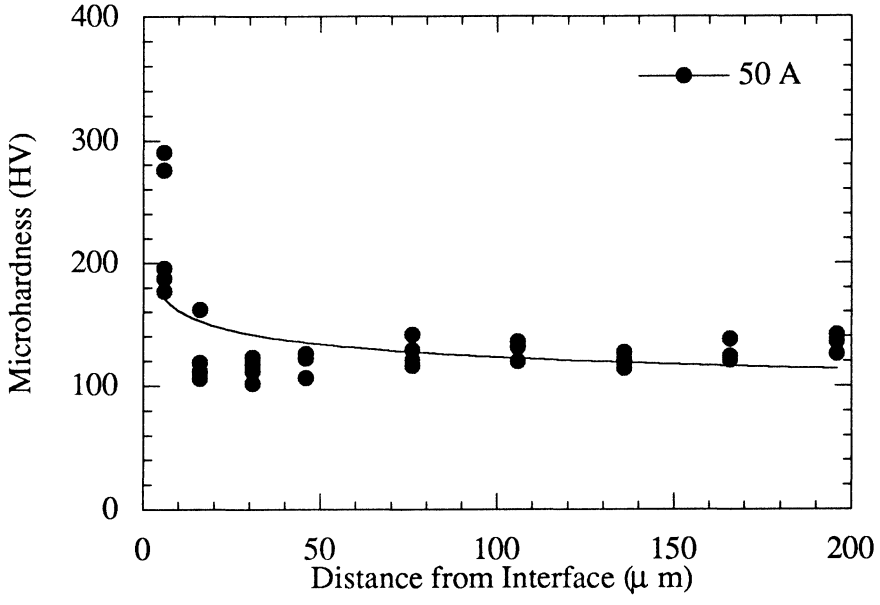

Figure 41. Variation of microhardness for the Cu-15vol.%Cr with the distance from the sliding interface after lubricated electrical sliding for 60 min under a normal pressure of 0.62 MPa and at a speed of 3.87 m s^{-1}.

4.5 Wear Mechanism of Electrical Sliding

During the electrical sliding, different material removal mechanisms were introduced, such as arc melting and arc erosion. The electrical arc emitted from the interface eroded both the composite pin and the steel disk. Figure 42 shows the arc eroded surface of the Cu-15vol.%Cr pin after dry electrical sliding for 60 min under a normal pressure of 0.31 MPa, at a speed of 4.16 m s^{-1}, and under an electrical current of 50 A. Features of erosion pits and cracks caused by arc melting and arc erosion existed on the worn surface.

Figure 42. Electrical arc eroded surface of the Cu-15vol.%Cr, after dry electrical sliding for 60 min under a normal pressure of 0.31 MPa, at a speed of 4.16 m s^{-1}, and under an electrical current of 50 A. Arrow shows the sliding direction.

A thick film was developed on the worn surface. SEM micrographs in Fig. 43 show three different surface areas on the Cu-15vol.%Cr *in situ* composite after dry

electrical sliding for 60 min under a normal pressure of 0.31 MPa, at a speed of 4.16 m s^{-1}, and with an electrical current of 40 A. Figure 43 (a) shows an arc melting characteristic and a thick film over the worn surface. Deep arc erosion pits can be observed on Fig. 43 (b) with some dendrite-like structure. No plastic deformation feature on the worn surface can be observed from Figs. 43 (a) and (b). The surface was covered by a thick layer formed as a result of arc erosion, melting and sliding. In the area shown in Fig 43 (c), wear debris were attracted onto the worn surface and plastic deformation could be seen.

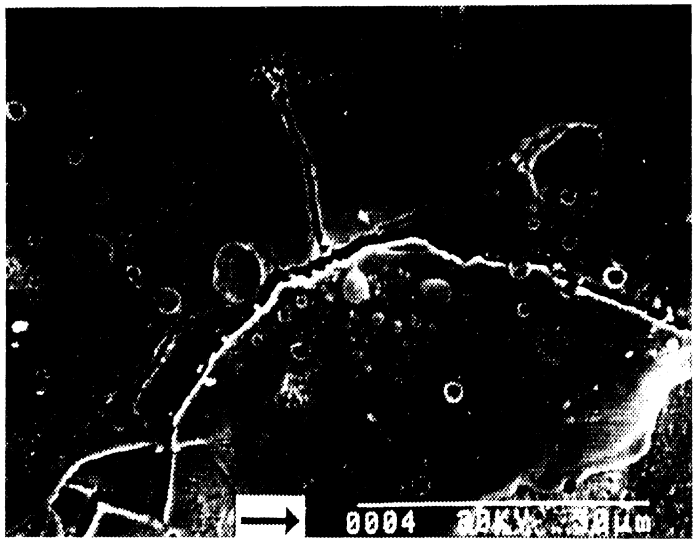

Figure 43. SEM micrographs of the Cu-15vol.%Cr, after dry electrical sliding for 60 min under a normal pressure of 0.31 MPa, at a speed of 4.16 m s^{-1}, and under an electrical current of 40 A. (a) surface crack; (b) arc eroded pits, and (c) wear debris attached on the surface. Arrow shows the sliding direction.

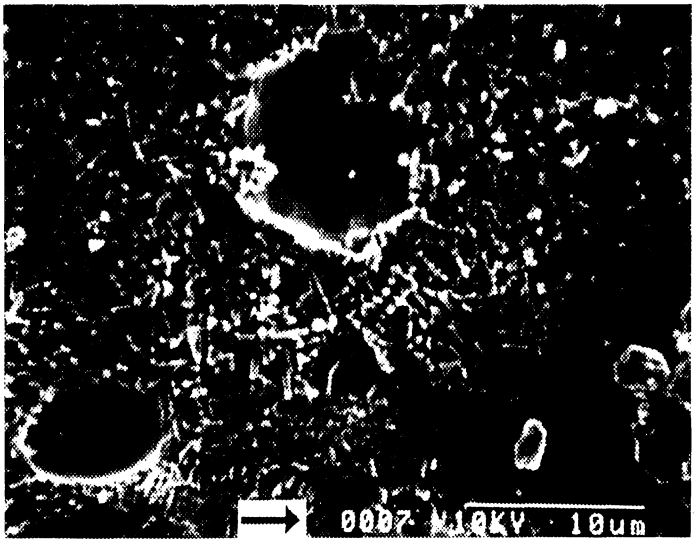

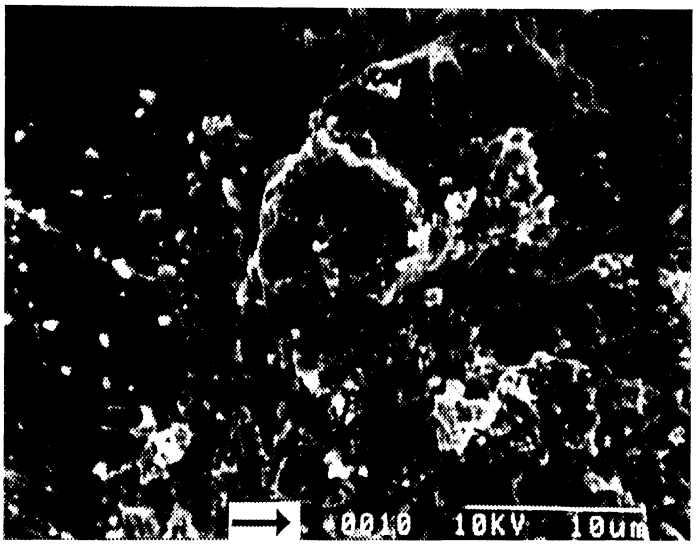

Figure 43. (Continued)

Figure 44 shows the wear debris collected from a dry electrical sliding test under a normal pressure of 0.31 MPa, at a speed of 3.33 m s^{-1}, and under an electrical current of 30 A. The wear debris were molded into a polymeric matrix before polishing. Spherical droplets and wear debris of irregular shape were shown in the microphotograph. The wear debris had a microstructure similar to but was less extensively deformed than that of the refined layer. The spherical droplets had a dendrite-like microstructure that is consistent with what was shown in Fig. 43 (b).

Figure 44. Wear debris collected from a dry electrical sliding test under a normal pressure of 0.31 MPa, at a speed of 3.33 m s^{-1}, and under an electrical current of 30 A.

Figure 45 shows the arc eroded sliding tracks on a steel disk after dry electrical sliding for 60 min under a normal pressure of 0.31 MPa, at a sliding speed of 4.16 m s^{-1}, and under an electrical current of 10 A. The same features as those on the worn surface of the Cu-15vol.%Cr *in situ* composite can be observed, *i.e.*, arc melting and arc erosion pits. However, plastic deformation and plowing can still be observed from the micro-photograph (near the right edge in Fig. 45).

Figure 45. Electrical arc eroded wear surface of the hardened steel disk, after dry electrical sliding for 60 min under a normal pressure of 0.31 MPa, at a speed of 4.16 m s^{-1}, and under an electrical current of 10 A. Arrow shows the sliding direction.

The bulk temperature rise caused by frictional heating, plastic deformation, Joule heating, and arcing would soften both the Cu-15vol.%Cr pin and the steel disk. Because the thermal conductivity of Cu-15vol.%Cr is higher than that of the AISI 52100 steel disk, the highest temperature would lie in the side of the steel (McNab, 1980).

Examination on steel disks after wear tests indicated that a deeply cut and severely oxidized sliding track existed on the steel disks. The degree of plowing increased with increasing electrical current and the steel was transferred to the worn surface of the composite pin.

When an electrical current was applied across the sliding interface, arc erosion occurred and temperature increased drastically. As a result, both the composite pin and steel disk were softened, which resulted in a lower coefficient of friction and a decreased thickness of the subsurface deformation layer. Because of the arc erosion, the steel disk was severely eroded and significant number of steel particles were back transferred to the composite pin during dry electrical sliding. A hardened surface layer was formed on the composite, which was composed of refined composite structure, oxides, wear debris, arc melted droplets and steel particles. Because of the hardened layer, the wear rate of the composite decreased with increasing electrical current whereas the steel disk was deeply cut on the sliding track.

Under lubricated electrical sliding, the composite was damaged or worn in a way similar to dry sliding. However, because the coefficient of friction is much lower at lubricated sliding and the lubricant film provides protection from oxidation, the degree of damage on both the composite and the steel disk is much less. When electrical current was increased, the bulk temperature increased. As a result, the effectiveness of the lubricant is reduced significantly. Consequently, the thickness of the subsurface deformation layer and the wear rate increased with increasing electrical current.

Conclusions

The following conclusions were made from the study of electrotribological behavior of deformation-processed Cu-15vol.%Cr *in situ* composite.

(1) The average coefficient of friction decreased with increasing electrical current under dry conditions. However, the average coefficient of friction increased with increasing electrical current under lubricated conditions. The lubricated electrical sliding had much lower coefficient of friction than dry electrical sliding.

(2) On dry electrical sliding, there are no significant effects of normal pressure and sliding speed on coefficient of friction. Under lubricated electrical sliding, the coefficient of friction decreased with increasing normal pressure, but it did not change significantly with sliding speed.

(3) Both static and dynamic interfacial contact resistances decreased slightly with increasing normal pressure. The dynamic interfacial contact resistance decreased with increasing electrical current. The openness of circuit decreased with increasing normal pressure, increased with increasing sliding speed and electrical current.

(4) The bulk temperature increased with increasing electrical current for both dry and lubricated conditions.

(5) The non-electrical wear rate of the composite increased with increasing normal pressure and decreased with increasing sliding speed. Electrical wear rate decreased with increasing electrical current under dry electrical sliding, whereas wear rate increased with increasing current under lubricated electrical sliding. Lubricated electrical sliding had a much lower wear rate than dry sliding.

(6) The effects of normal pressure and sliding speed on wear rate of the composite under both dry and lubricated electrical sliding are dependent upon the level of electrical current.

(7) The sliding-induced subsurface deformation occurred not only in the sliding direction but also in the lateral directions perpendicular to the sliding direction. The complex deformation mode was revealed clearly by the morphological change of the ribbon-like filaments. Experiments showed that the frictional forces produced a lateral flow that was largest at the surfaces of the specimen.

(8) The thickness of the subsurface deformation layer increased with increasing normal pressure and sliding speed under dry non-electrical conditions. Thickness of subsurface deformation layer decreased with increasing electrical current under dry conditions, whereas the thickness increased with increasing electrical current under lubricated electrical sliding.

(9) SEM analysis showed plastic deformation flow on the worn surface and illustrated that the surface deformation flow was affected by wear particles back transferred onto the surface on dry non-electrical sliding.

(10) A hardened surface layer was observed after electrical sliding, which consisted of refined structure, oxides, back transferred steel and arc eroded droplets. The hardened surface layer and less damage on the subsurface layer were accounted for reduction in wear rate as electrical current was applied.

References

ASM (1992). Metals Handbook (10th ed., Vol. 3, pp. 2.172-2.173). Materials Park, Ohio: ASM International.

Bevk, J., Harbison, J. P., & Bell, J. L. (1978). Anomalous increase in strength of *in situ* formed Cu-Nb multifilamentary composites. J. Appl. Phys., 49(12), 6031-6038.

Chen, Z., Liu, P., Verhoeven, J. D. and Gibson, E. D. (1995). Sliding wear behavior and microstructure change of deformation-processed Cu-20vol.%Nb *in situ* composite, Wear, 181-183, 263-270.

Chumbley, L. S., Downing, H. L., Spitzig, W. A., & Verhoeven, J. D. (1989). Electron microscopy observation of an *in-situ* Cu-Nb composite. Materials Science Engineering, A: Structural, 117(1), 59-65.

Courtney, T. H. (1991). Strengthening behavior of *in situ* composites. In R. K. Everett & R. J. Arsenault (eds.), Metal matrix composites: Mechanisms and properties (pp. 101-131). Boston: Academic Press.

Donaldson, A. L., Lehr, F. M., & Christiansen, M. (1988). Performance of *in situ* copper alloys as electrodes in high current, high energy switches. SPIE O-E/Lase Conference, 1st section (Space Power and Power Conditioning), Los Angels, California, January 10-15, 1988.

Downing, H. L., Verhoeven, J. D., & Gibson, E. D. (1987). The emissivity of etched Cu-Nb *in situ* alloys. J. Appl. Phys. 61(7), 2621-2625.

Frommeyer, G., & Wassermann, G. (1975). Microstructure and anomalous mechanical properties of *in situ* produced silver-copper composite wires. Acta Metallurgica, 23(11), 1353-1360.

Fujiwara, O., Tsukamoto, S., & Azakami, T. (1990). Intrinsic properties of discontact phenomena occurring in sliding contacts. Journal of Institute of Electronics, Information, Communication Engineering, J73-C-II(12), 852-858.

Funkenbusch, P. D., & Courtney, T. H. (1985). On the strength of heavily cold worked *in situ* composites. Acta Metallurgica, 33(5), 913-922.

Funkenbusch, P. D., Courtney, T. H., & Kubisch, D. G. (1984). Fabricability of and microstructural development in cold worked metal matrix composites. Scripta Metallurgica, 18, 1099-1104.

Hardwick, D. A., Rhodes, C. G., & Fritzemeier, L. C. (1993). The effect of annealing on the microstructure and mechanical properties of Cu-X microcomposites. Metallurgical Transactions A, 24A(1), 27-34.

Hornbogen, E. (1985). Description of wear of materials with isotropic and anisotropic microstructure. In K. C. Ludema (ed.), Wear of Materials 1985, (pp. 477-484). New York: The American Society of Mechanical Engineers.

Johnson, J. L., & Schreurs, J. (1982). High current brushes VIII: Effect of electrical load. Wear, 78, 219-232.

Kim, S. T. (1993). Processing of copper-7v/o chromium alloy: optimum processing for combination of strength and electrical conductivity. Master's thesis, Iowa State University, Ames, Iowa.

Liu, P., Bahadur, S., & Verhoeven, J. D. (1993a). Further investigation on the

tribological behavior of Cu-20%Nb *in situ* composite. Wear, 162-164, 211-219.

Liu, P., Bahadur, S., & Verhoeven, J. D. (1993b). The mechanical and tribological behavior of Cu-Nb *in situ* composites. Wear, 166 , 133-139.

Liu, P., Bahadur, S., & Verhoeven, J. D. (1994). Electrical sliding friction and wear behavior of Cu-Nb *in situ* composites. IEEE Transactions on Components, Packing and Manufacturing Technology-*Part A*, 17, 616-623.

Lysonski, R., Haberl, J., Denton, L. R., File, D., Anderson, G., Williams J., Morey, R., Reed, W., & Breindel, H. (1990). Test system for measurement of noise and coefficient of friction as a screen for potential lubricants in sliding electrical contacts. In Electrical Contacts--1990 (pp. 269-277), New York: IEEE.

Matthews, F. L., & Rawlings, R. D. (1994). Composites materials: Engineering and science. London: Chapman & Hall.

McNab, I. R. (1980). Recent advances in electrical current collection. Wear, 59, 259-276.

Myshkin, N. K., & Konchits, V. V. (1992). Friction and wear of metal-composite electrical contacts. Wear, 158, 119-140.

Nayeb-Hashemi, H., & Lee, K. (1993). Friction and wear behavior of Cu-Nb microcomposite produced by powder metallurgy. In M. H. Attia & R. Komanduri (eds.), Contact problems and surface interaction in manufacturing and tribological systems (pp. 263-267). New York: ASME.

Okada, K., Baba, S., & Yoshida, M. (1989). Studies on electrical contact lubricants for metal brushes. In Electrical contacts and electromechanical components--Proceedings of the international conference on electrical contacts and electromechanical components (pp. 79-84). Beijing: International Academic Publisher.

Persad, C., Sparks, S. C., Moore, D., Schmerling, M., Eliezer, Z., Gully, J., & Carnes, R. (1990). Advanced composite materials for high-performance electrotribological applications. In P. K. Rohatgi, P. J. Plau, & C. S. Yust (eds.), Tribology of composite materials. (pp. 203-216). Materials Park, Ohio: ASM International.

Pourrahimi, S., Nayeb-Hashemi, H., & Foner, S. (1992). Strength and microstructure of powder metallurgy processed restacked Cu-Nb microcomposites. Metallurgical Transactions A, 23A, 573-586.

Raabe, D., Ball, J., & Gottstein, G. (1992). Rolling texture of a Cu-20%Nb composite. Scripta Metallurgica et Materialia, 27(2), 211-216.

Renaud, C. V., Gregory, E., & Wong, J. (1988). Development and application of high strength, high conductivity CuNb *in situ* composite wire and strip. In A. F. Clark & R. P. Reed (eds.), Advances in cryogenic engineering materials, 34 (pp. 435-442). Plenum Press: New York.

Rigney, D. A. (1988). Sliding wear of metals. Ann. Rev. Mater. Sci., 18, 141-163.

Rohatgi, P. K., Liu, Y., & Ray, S. (1993). Friction and wear of metal-matrix composites. In Materials handbook, 17, (pp. 801-811). Materials Park, Ohio: ASM International.

Schreurs, I., Johnson, J. L., & McNab, I. R. (1980). High-current brushes, Part

VI: Evaluation of slip ring surface films. IEEE Trans. Components, Hybrids, Manuf., Technol., CHMT-3, 83-88.

Spitzig, W. A., Downing, H. L., Laabs, F. C., Gibson, E. D., & Verhoeven, J. D. (1993). Strength and electrical conductivity of a deformation-processed Cu-5%Nb composite. Metallurgical Transactions A, 24A(1), 7-14.

Spitzig, W. A., & Krotz, P. D. (1987). A comparison of the strength and microstructure of heavily cold worked Cu-20%Nb composites formed by different melting procedures. Script Metallurgica, 21, 1143-1146.

Spitzig, W. A., & Krotz, P. D. (1988). Comparison of the strengths and microstructure of Cu-20%Ta and Cu-20%Nb *in situ* composites. Acta Metallurgica, 36(7), 1709-1715.

Spitzig, W. A., Pelton, A. R. , & Laabs, F. C. (1987). Characterization of the strength and microstructure of heavily cold worked Cu-Nb composites. Acta Metallurgica, 35, 2427-2442.

Spitzig, W. A., & Reed, L. K. (1989). Temperature and strain rate dependence of the strength of heavily cold-drawn copper, niobium and Cu-20%Nb. Materials Science and Engineering, A 111, L13-L17.

Trybus, C. L., & Spitzig, W. A. (1989). Characterization of the strength and microstructural evolution of a heavily cold rolled Cu-20%Nb composite. Acta Metallurgica, 37(7), 971-981.

Verhoeven, J. D., Chueh, S. C., & Gibson, E. D. (1989). Strength and conductivity of *in-situ* Cu-Fe alloys. Journal of Materials Science, 24(5), 1748-1752.

Verhoeven, J. D., Chumbley, L. S., Laabs, F. C., & Spitzig, W. A. (1991). Measurement of filament spacing in deformation processed Cu-Nb alloys. Acta Metallurgica et Materialia, 39(11), 2825-2834.

Verhoeven, J. D., Gibson, E. D., Schmidt, F. A., & Finnemore, D. K. (1980). Preparation of Cu-Nb alloys for multifilamentary *in situ* superconducting wire. Journal of Materials Science, 15, 1449-1455.

Verhoeven, J. D., Spitzig, W. A. , Jones, L. L., Downing, H. L., Trybus, C. L., Gibson, E. D., Chumbley, L. S., Fritzemeier, L. G., & Schnittgrund, G. D. (1990). Development of development processed copper-refractory metal composite alloys. J. Mater. Engineering, 12, 127-139.

Verhoeven, J. D., Spitzig, W. A., Schmidt, F. A. Krotz, P. D., & Gibson, E. D. (1989). Processing to optimize the strength of heavily drawn Cu-Nb alloys. Journal of Materials Science, 24(3), 1015-1020.